Case Studies in Thermal Engineering 77 (2026) 107589

Contents lists available at ScienceDirect

Case Studies in Thermal Engineering

journal homepage: www.elsevier.com/locate/csite

Optimizing building heating demand through solar-air temperature integration: A comprehensive analysis of free heating potential and energy savings

Ali Keçebaş [a], Hongwei Wu [b,*], Mustafa Ertürk [c], C Ahamed Saleel [d,e]

[a] Department of Energy Systems Engineering, Technology Faculty, Muğla Sıtkı Koçman University, Menteşe, 48000, Muğla, Turkey
[b] School of Physics, Engineering and Computer Science, University of Hertfordshire, Hatfield, Hertfordshire, AL10 9AB, United Kingdom
[c] Department of Mechanical Engineering, Technology Faculty, Sakarya University of Applied Sciences, 54187, Serdivan, Sakarya, Turkey
[d] Department of Mechanical Engineering, College of Engineering, King Khalid University, PO Box 394, Abha, 61421, Saudi Arabia
[e] Center for Engineering and Technology Innovations, King Khalid University, Abha, 61421, Saudi Arabia

GRAPHICAL ABSTRACT

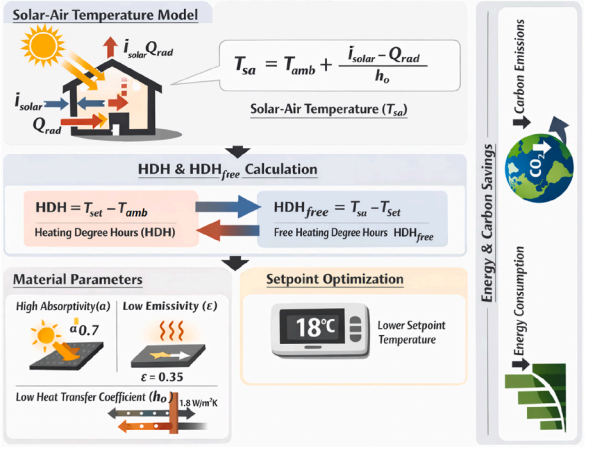

ARTICLE INFO

Keywords:
Energy efficiency in buildings

ABSTRACT

This study presents an innovative methodology for estimating building heating demand by incorporating the solar-air temperature concept into heating degree hour (HDH) and free heating

* Corresponding author.
E-mail address: h.wu6@herts.ac.uk (H. Wu).

https://doi.org/10.1016/j.csite.2025.107589
Received 11 November 2025; Received in revised form 20 December 2025; Accepted 23 December 2025
Available online 24 December 2025

Free heating degree hours
Free heating potential
Heat transfer optimization
Passive heating systems
Solar-air temperature

degree hour (HDH_{free}) calculations. Unlike conventional methods that rely solely on ambient temperature, this approach integrates for solar radiation and radiative heat loss, providing a more accurate assessment of heating demand and free heating potential. The results indicate that lowering indoor setpoint temperatures to 18 °C can reduce annual heating demand by 25–40 %, while optimizing the heat transfer coefficient (h_o = 1.8 W/m^{2}K) results in an 82 % increase in HDH_{free}. This increase is attributed to a reduction in conductive heat losses through the building envelope, allowing solar gains to be retained for a longer period while maximizing passive heating effectiveness. Lower h_o values also minimize radiative and convective heat losses, enabling the absorbed solar energy to remain within the building for an extended duration, ultimately enhancing free heating efficiency. The study also highlights the importance of material properties, with higher solar absorptivity (0.7) leading to a 40 % improvement in energy savings and lower surface emissivity (0.35) contributing to better heat retention. The methodology was validated using data from Muğla, Turkey, demonstrating significant energy cost savings and carbon footprint reductions, especially in electricity-based systems. Future research should focus on refining the solar-air temperature model by incorporating building-specific variables and expanding its application to different climates. This approach offers a valuable contribution to sustainable building design by optimizing passive heating and reducing reliance on mechanical systems.

1. Introduction

The growing demand for energy-efficient and sustainable buildings has catalyzed the development of innovative heating systems that decrease reliance on conventional fossil fuels [1]. As global energy consumption rises, passive heating technologies, which harness solar energy to lower heating loads, have become essential in reducing both energy demand and greenhouse gas emissions [2]. This approach is particularly effective in regions with significant seasonal variations, where solar energy can partially or fully replace mechanical heating during specific periods [3]. Accurate assessment of a building's heating needs is crucial for optimizing energy consumption and reducing operational costs [4]. Proper energy evaluations facilitate the implementation of efficient solutions such as insulation, renewable energy systems, and smart building technologies, which contribute to lowering both energy bills and carbon footprints [5]. Additionally, optimizing energy use enhances indoor comfort and helps meet regulatory standards, making buildings more resilient to environmental conditions and fluctuations in energy prices [6].

In Europe, passive heating has gained significant importance due to strict energy efficiency regulations [7]. Buildings account for nearly 40 % of the EU's total energy consumption, with heating comprising around 70 % of that demand [8]. Studies show that passive heating strategies—such as improved insulation and optimized solar gain—can lower heating energy consumption by 20–30 %, depending on the climate and building design [9]. Countries like Germany and Sweden have achieved energy savings of up to 60–90 % through the adoption of passive house standards [10]. In Mediterranean countries, passive heating measures contribute to a 15–25 % reduction in heating energy consumption, offering significant potential for energy savings during the cooler months [2]. The ability of passive heating to diminish dependency on active heating systems makes it a key factor in sustainable building design [11]. By leveraging natural heat sources, passive heating reduces operational costs and carbon emissions. During the design phase, understanding how to optimize passive heating—through factors like building orientation, insulation, and material properties—enhances the accuracy of energy demand predictions, leading to more sustainable and cost-effective buildings [12].

The degree-hour methodology plays a crucial role in estimating heating demand for passive heating [13]. By calculating the difference between outdoor and indoor setpoint temperatures, this approach provides a more accurate evaluation of heating energy requirements [14]. Incorporating solar-air temperature adjustments into the degree-hour method further refines these calculations, enabling the design of buildings that significantly minimize the need for active heating systems while reducing energy consumption and costs [15]. Several studies have focused on determining the optimal insulation thickness to improve energy efficiency in buildings. Bolattürk [16] and Yu et al. [17] analyzed the effect of insulation thickness on energy savings in different climatic zones. Bolattürk [16] applied the degree-hour method in Turkey's warmest regions, recommending insulation thicknesses of 1.6–3.8 cm to achieve energy savings, with payback periods of approximately 3–5 years. Similarly, Yu et al. [17] determined the optimal insulation thickness for roofs in China's hot summer and cold winter regions, finding thicknesses ranging from 0.065 to 0.187 m, with life cycle savings of up to \$112.2/m^2. Aktemur et al. [18] extended this analysis by factoring in solar radiation, wall orientations, and insulation material types. They calculated the optimal thickness for various materials and wall configurations in Erzincan, Turkey, concluding that the thickness varied based on orientation, ranging from 0.0318 m for south-facing walls to 0.0638 m for north-facing walls.

Numerous studies have attempted to characterize building cooling loads using variations of degree-day and degree-hour methodologies, yet most have failed to fully incorporate radiative phenomena or dynamic atmospheric classifications. For example, Wati et al. [19] and Zhou et al. [20] used conventional temperature-based indicators to estimate cooling requirements without accounting for solar radiation effects. Alola et al. [21] incorporated climate-driven CDD-HDD variability but did not operationalize radiative load contributions. He et al. [22] evaluated envelope-level improvements but remained constrained to static ambient temperature assumptions. Huang and Zhai [23], Panchabikesan et al. [24], and Shen et al. [25] addressed regional or material-specific thermal strategies but lacked a unified model that considers emissivity and sky-dependent thermal behavior. Ustaoglu et al. [26] introduced climate zones into the CDH framework but did not differentiate sky conditions dynamically. Yan et al. [27], Yang et al. [28], and Zhang

et al. [29] expanded thermal modeling with experimental or empirical insight, yet did not formalize solar-air temperature as a predictive metric. Shakir et al. [30] used machine learning to forecast loads but omitted physical thermal interactions like surface radiative heat exchange. Yang et al. [31], Kheiri et al. [32], and Li et al. [33] advanced simulation-based assessments, but relied on ambient-only or time-averaged climate indicators. Sulzer et al. [34], Wong et al. [35], and Fellah et al. [36] provided valuable insights into diurnal variations and energy prediction, yet none integrated a ΔT-based classification linked to free cooling estimation. Ozturan and Seyhan [37] and Palma et al. [38] analyzed insulation performance and solar-air dynamics, but not in the context of CDH modeling. Breteau et al. [39], Evola et al. [40], Fan et al. [41], and Fellah et al. [42] made notable contributions to urban-scale or ML-augmented cooling assessments; however, their models did not account for the coupled effects of emissivity, surface radiation, and hourly sky-state identification. Zhou et al. [43] explored PCM-enhanced envelope systems, and Zmeureanu et al. [44] investigated building inertia and responsiveness, yet both lacked methodological frameworks to assess free cooling windows on a radiatively active basis.

The degree-hour methodology is fundamental to calculating heating and cooling loads. Ghiaus [45] demonstrated the accuracy of the load curve method in predicting energy consumption, showing a margin of error of less than 5 % error for both heating and cooling. De Rosa et al. [46] refined this approach by incorporating solar irradiation into a simplified energy demand model, achieving an impressive 99 % accuracy when validated against established simulation tools like EnergyPlus. Harvey [47] and Lyu et al. [48] applied variations of the degree-hour method to account for climate-specific factors. Harvey [47] introduced modified heating-degree-day (HDD) and cooling-degree-day (CDD) indices to estimate building loads with greater precision, particularly in multi-unit residential buildings. Lyu et al. [48] proposed a revised degree-hours method that assessed the performance of natural energy systems such as mechanical ventilation and ground heat exchangers in different climates, achieving energy savings of up to 60 %.

Several studies have explored passive strategies for reducing heating and cooling loads. Zhang et al. [49] examined on building materials' thermophysical properties, identifying that materials with thermal capacities above 50 MJ/m^3°C were ideal for free-cooling, while capacities of 100 MJ/m^3°C were required for year-round free-heating and cooling. Pothof et al. [50] presented a data-driven optimization method to optimize heating supply temperatures in residential buildings, reducing heating loads by using lower supply temperatures while maintaining thermal comfort. Roshan et al. [51] and Huo et al. [52] focused on climate-specific applications. Roshan et al. [51] developed new threshold temperatures for Iran's climatic zones, optimizing energy use by adjusting comfort levels in heating and cooling. Huo et al. [52] introduced an index to assess free-running buildings' potential, finding that cities like Kunming had nearly 100 % of summer hours within comfort ranges. Adaptive comfort standards offer another effective approach for optimizing energy consumption. McGilligan et al. [53] developed the Adaptive Comfort Degree-Day metric to compare adaptive comfort standards like EN15251 and ASHRAE 55. Their results showed that applying European standards could lead to significant energy savings under projected UK climate conditions. Zhang et al. [49] and Hu et al. [54] extended this concept by comparing occupant thermal needs under different heating modes, highlighting substantial energy savings in fee-charged heating systems.

Integrating solar-air temperature adjustments into energy models can significantly improve the accuracy of heating demand calculations. Yu et al. [17] applied solar-air degree-hour calculations to optimize insulation thickness for roofs, demonstrating the substantial energy-saving potential in China's climate. Keçebaş et al. [55] further explored this concept by incorporating exergy-based calculations into the degree-hour method. Their study showed that a 1 °C increase in ambient temperature led to a 14 % rise in heating demand, while exergy-based degree-hours reduced energy requirements by up to 97.5 % compared to traditional calculations. Several studies have quantified the economic and environmental impacts of energy efficiency measures. Bolattürk [16] and Aktemur et al. [18] demonstrated the cost-effectiveness of optimal insulation, with payback periods of less than five years and considerable life cycle savings. Pothof et al. [50] and Hu et al. [54] provided evidence of notable energy savings through optimized heating systems, with potential reductions in energy use and carbon emissions of up to 55 %. Previous studies have explored variations of the solar-air temperature concept for different building energy applications. However, these studies have not specifically integrated solar-air temperature into the conventional HDH model, which represents a key contribution of this research. Traditional methods for estimating building heating demand predominantly rely on the HDH approach, which considers the difference between indoor setpoint temperature and ambient temperature. However, these methods often overlook the dynamic impact of solar radiation on heating loads. Prior studies [16–18,45–54] have investigated the relationship between insulation thickness and energy savings in different climatic zones. However, they did not incorporate solar radiation effects into their models. Similarly, some studies [16–18,50,54,55] attempted to refine degree-hour methodologies by incorporating solar irradiation, but their approaches primarily used fixed coefficients without capturing the real-time fluctuations in solar heat gains. This study aims to address these limitations by developing a methodology that integrates the solar-air temperature (T_{sa}) concept into heating degree hour calculations, allowing for a more accurate prediction of heating demand and free heating potential.

This study presents a notable contribution to the existing literature by advancing the methodology for estimating heating demand through the integration of T_{sa}, which has not been extensively applied in prior studies. Unlike conventional methods that rely solely on ambient temperature, this approach incorporates the effects of solar radiation, providing a more precise prediction of heating demand and free heating potential. The scientific innovation of the study lies in its ability to quantify the contribution of solar gains to passive heating systems, offering a comprehensive framework that enhances energy savings and reduces reliance on mechanical heating. Furthermore, the methodology proposed here not only addresses the limitations of traditional heating degree-hour calculations but also introduces practical solutions for optimizing building performance in regions with distinct seasonal characteristics. By bridging the gap between theoretical modeling and real-world application, this research provides critical insights into sustainable building design and contributes to the broader effort to reduce energy consumption and greenhouse gas emissions. The primary objective of this study is to enhance the accuracy of heating demand estimation by incorporating T_{sa} into HDH framework. By integrating solar radiation and radiative heat losses into the heating load calculations, this approach provides a more holistic assessment of free heating

potential. Specifically, the study seeks to answer the following research questions:

- What impact does the incorporation of T_{sa} into HDH calculations have on HDH_{free} compared to conventional ambient temperature-based models?
- How do building material properties, such as solar absorptivity and surface emissivity, affect free heating potential?
- How can different indoor setpoint temperatures and climatic conditions be optimized to maximize free heating efficiency while minimizing mechanical heating demand?

2. Methodology

2.1. Calculation of heating demand

The total annual heating demand of a building refers to the overall amount of energy required to maintain indoor comfort conditions throughout a year. This energy demand arises when outdoor temperatures fall below the specified indoor setpoint temperature, requiring the heating system to compensate for heat losses. Several factors influence heating demand, including insulation quality, outdoor temperatures, indoor temperature setpoints, and solar radiation.

The cumulative heating demand over a year is calculated as the sum of hourly heat losses throughout the entire period. This value represents the total energy consumption required to sustain indoor comfort conditions. The total heating energy demand over a year is expressed as [55]:

$$\dot{E}_{heating} = \sum_{t=1}^{8760} \frac{\dot{Q}_{heating}(t)}{\eta} \tag{1}$$

where, η represents the efficiency of the heating system. t denotes time (hour), with 8760 corresponding to the total number of hours in a year (365 days × 24 h). $\dot{Q}_{heating}(t)$ is the hourly heating demand, calculated as follows:

$$\dot{Q}_{heating}(t) = \begin{cases} 0 & \text{if } T_{amb}(t) \geq T_{setpoint} \\ \dot{Q}_{loss}(t) & \text{if } T_{amb}(t) < T_{setpoint} \end{cases} \tag{2}$$

where $T_{amb}(t)$ and $T_{setpoint}$ represent the outside air temperature and the indoor setpoint (comfort) temperature, respectively, for a building requiring heating. $\dot{Q}_{loss}(t)$ is the heat loss during a given hour.

Heat loss occurs when there is a temperature difference between the inside of the building and the outside ambient temperature. The heating system must compensate for these heat losses to maintain the desired indoor temperature. The hourly heat loss is calculated using the following formula:

$$\dot{Q}_{loss}(t) = UA \sum_{t=1}^{8760} \left[T_{setpoint} - T_{amb}(t)\right]^{*} \quad \text{for } T_{amb}(t) < T_{setpoint} \tag{3}$$

where, UA denotes the overall heat transfer coefficient and surface area of the building envelope, and the asterisk (*) indicates that only positive values are considered.

The total heating demand for a heating system is calculated using traditional Heating Degree Hours (HDH), which helps determine the hours during which heating is needed. To quantify the heating potential based on the outside ambient temperature, HDH is calculated as:

$$HDH = \sum_{t=1}^{8760} \left[T_{setpoint} - T_{amb}(t)\right]^{*} \quad \text{for } T_{amb}(t) < T_{setpoint} \tag{4}$$

2.2. Solar-air temperature model

This methodology extends the fundamental principles of air-based free heating by incorporating the concept of solar-air temperature ($T_{sa}(t)$) instead of ambient temperature. The use of $T_{sa}(t)$ allows for a more accurate estimation of heating capacity and energy savings by accounting for the impact of solar radiation. Unlike conventional approaches that solely rely on ambient temperature, this study integrates $T_{sa}(t)$, which accounts for both solar heat gains and radiative losses, thereby enhancing the accuracy of heating demand estimations. This methodology ensures a more realistic and dynamic representation of passive heating potential by incorporating key environmental factors. The formula for $T_{sa}(t)$ is given as [56]:

$$T_{sa}(t) = T_{amb}(t) + \frac{\alpha I}{h_o} - \frac{\varepsilon\sigma\left(T_{amb}^4 - T_{sky}^4\right)}{h_o} \tag{5}$$

where $T_{sa}(t)$ represents the hourly solar-air temperature, $T_{amb}(t)$ stands for the hourly outside ambient temperature, α signifies the solar absorptivity of the surface, I represents the solar radiation incident on the surface, ε represents the surface emissivity, and σ is the Stefan-Boltzmann constant. Within this context, $[\alpha I / h_o]$ describes the impact of solar heat gain on the opaque surface, while the term $\left[\varepsilon\sigma\left(T_{amb}^4 - T_{sky}^4\right)/h_o\right]$ accounts for temperature corrections in radiation heat transfer when $T_{sky} \neq T_{amb}$. According to the ISO 13790

standard [57], T_{sky} is the sky temperature, typically 7–13 °C lower than the ambient temperature depending on the climate. h_o is the combined convection and radiation heat transfer coefficient, calculated as:

$$h_o = h_{o,conv} + h_{o,rad} \tag{6}$$

where $h_{o,rad}$ is the radiation heat transfer coefficient, calculated as [58]:

$$h_{o,rad} = \varepsilon\sigma\left(T_{amb}^2 + T_{sky}^2\right)\left(T_{amb} + T_{sky}\right) \tag{7}$$

The selected external heat-transfer coefficients h_o correspond to steady-state façade convection conditions widely adopted in simplified heat-loss assessments and are consistent with ISO 6946 [59] and ASHRAE [60] guidelines for representative outdoor surface coefficients; therefore, these fixed values are employed here to isolate the sole influence of convection on the solar-air temperature formulation and subsequent free heating degree hours' calculations.

2.3. Definition of free heating degree hours

Air-based free heating leverages solar energy to provide heating capacity when the outdoor temperature exceeds a certain setpoint. This process is typically represented using the solar-air temperature ($T_{sa}(t)$) and the indoor setpoint temperature ($T_{setpoint}$). To determine the hours when free heating is active and calculate the associated energy savings, the free heating capacity is evaluated based on the difference between $T_{sa}(t)$ and $T_{setpoint}$. Free heating operates when $T_{sa}(t)$ exceeds $T_{setpoint}$, allowing the building to rely on solar energy for heating, thus reducing the demand on mechanical systems.

Solar-air temperature $T_{sa}(t)$ enables for calculating the free heating capacity during hours when the solar gain helps meet indoor heating needs. The solar-air temperature equation, given in Eq. (5), is derived from the ISO 13790 Standard [57] and applied in building heat transfer studies such as Yu et al. [17]. This study extends the application of T_{sa} by integrating it into *HDH* formulation, providing an advanced methodology for passive heating assessment. Thus, the free heating capacity is defined as:

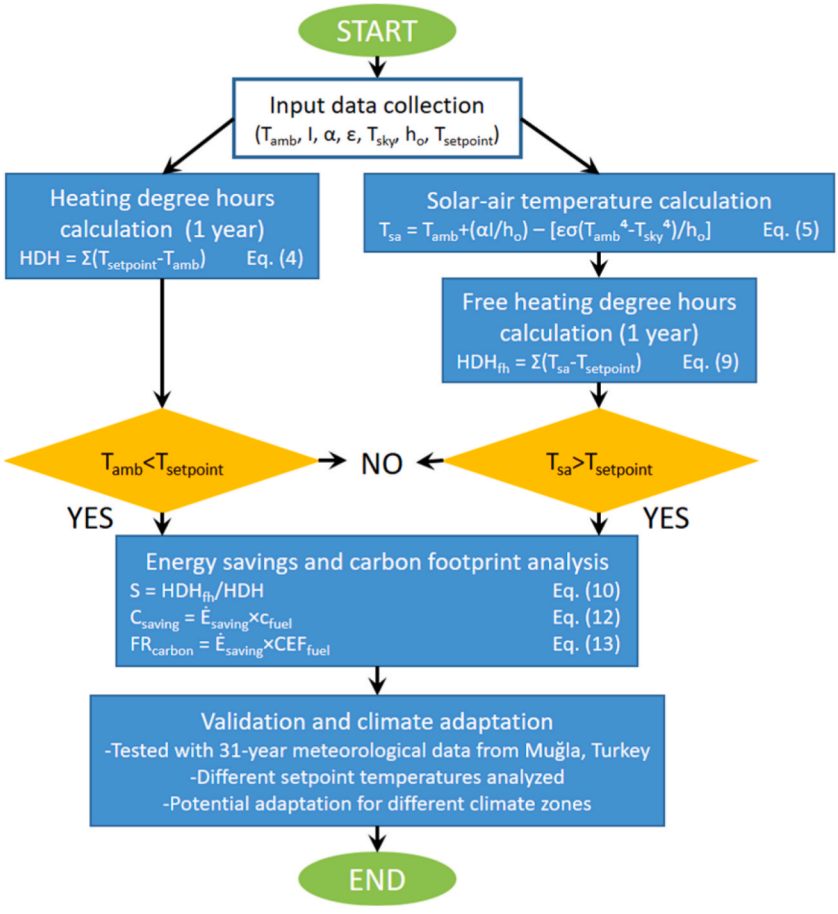

Fig. 1. Schematic representation of the methodology used in this study.

$$\dot{Q}_{fh}(t) = \begin{cases} 0 & \text{if } T_{sa}(t) \le T_{setpoint} \\ \dot{Q}_{gain}(t) & \text{if } T_{sa}(t) > T_{setpoint} \end{cases} \tag{8}$$

To quantify the heating potential based on $T_{sa}(t)$, the free heating degree-hours (HDH_{fh}) over a year are calculated as:

$$HDH_{fh} = \sum_{t=1}^{8760} \left[T_{sa}(t) - T_{setpoint}\right]^{*} \quad \text{for } T_{sa}(t) > T_{setpoint} \tag{9}$$

The HDH_{fh} formulation is applied exclusively to heating-dominated periods in which $T_{amb} < T_{setpoint}$, and it does not represent cooling-season behavior; therefore, the absorptivity values examined here refer solely to winter heating performance rather than year-round façade recommendations. Furthermore, the HDH_{fh} model operates as a steady-state, hourly framework and does not account for transient heat-storage effects such as time lag or phase shift. Consequently, the representation of heat gain in Eqs. (8) and (9) reflects only the immediate availability of free-heating potential.

The methodology developed in this study aims to optimize building heating demand estimation by incorporating solar-air temperature (T_{sa}) concept into traditional *HDH* calculations. Unlike conventional methods that solely rely on ambient temperature (T_{amb}), this approach integrates the effects of solar radiation and radiative heat losses to enhance the accuracy of heating demand predictions. In contrast to widely used energy simulation software (e.g., EnergyPlus, TRNSYS), which employs predefined climatic inputs and simplified solar heat gain models, this methodology dynamically integrates the effects of solar radiation and radiative heat losses into heating demand calculations. By incorporating real-time solar gain and radiative losses, this approach enhances the precision of free heating potential estimations, thereby reducing the reliance on mechanical heating systems and improving the accuracy of energy consumption predictions. Fig. 1 presents a schematic representation of this methodology, illustrating the step-by-step process. This figure outlines the main stages, including input data collection (T_{amb}, I, α, ε, T_{sky}, h_o, $T_{setpoint}$), *HDH* calculation, solar-air temperature estimation, free heating degree hours (HDH_{fh} or HDH_{free}) assessment, energy savings evaluation, and validation using real meteorological data from Muğla, Turkey.

2.4. Economic and environmental impact of free heating

If all other parameters (e.g., the total heat transfer coefficient, heat transfer area, and system efficiency) remain constant, energy savings due to free heating can be calculated based on degree-hours. The percentage energy saving derived from free heating is calculated as:

$$S = \frac{HDH_{fh}}{HDH} \tag{10}$$

Free heating potential is leveraged to reduce the load on the heating system, thereby achieving energy savings. By assessing the impact of free heating on the total annual energy savings, the economic value of these savings can be determined. The amount of energy saved is defined by HDH_{fh}, and this amount is calculated based on the proportion of free heating hours to total heating hours. The saved energy is expressed using the follow:

$$\dot{E}_{saving} = S \times \dot{E}_{heating} \tag{11}$$

where, $\dot{E}_{heating}$ represents the total annual heating energy demand. The economic value of these energy savings is then calculated by multiplying the saved energy, $\dot{E}_{saving}$, by the unit energy cost of any fuel, c_{fuel} ($/kWh):

$$C_{saving} = \dot{E}_{saving} \times c_{fuel} \tag{12}$$

This approach enables for the calculation of cost savings for building owners resulting from the use of free heating.

Free heating is the reduction in the carbon footprint achieved through energy savings. Particularly in systems where energy is derived from fossil fuels, the energy saved via free heating directly reduces carbon emissions. Carbon footprint reduction is calculated by multiplying the saved energy, $\dot{E}_{saving}$, by the carbon emission factor of any fuel, *CEF* (kg CO_2/kWh):

$$FR_{carbon} = \dot{E}_{saving} \times CEF_{fuel} \tag{13}$$

This quantifies the amount of CO_2 emissions prevented through the use of free heating.

2.5. Validation for a city

To validate the proposed methodology, a real-world case study was conducted using 31 years of high-resolution hourly meteorological data from Muğla, Turkey. By integrating empirical climate data, the study demonstrates the practical application of the solar-air temperature model in assessing free heating potential and optimizing heating demand calculations in real-world building scenarios. The case study further conf1irms that solar-assisted heating systems can significantly enhance energy efficiency, particularly in Mediterranean climates characterized by substantial seasonal solar variation. Muğla, located at approximately 37.22° N and 28.36° E, experiences a typical Mediterranean climate, with hot, dry summers and mild, wet winters [56]. The meteorological data used in this study, provided by the General Directorate of Meteorology [61], covered the period from 1984 to 2015 and included high-resolution hourly outdoor air temperature measurements ($T_{outside}(t)$). These data were fundamental for calculating heating degree hours (HDH)

and free heating degree hours (HDH_{free}).

Heating demand calculations in this study were performed on an hourly resolution, utilizing location-specific outdoor air temperature and solar radiation intensity data specific to Muğla, Turkey. To represent the heating season using representative days, a systematic selection process was employed wherein days were identified based on two primary criteria: (i) statistical representativeness of hourly temperature and solar radiation profiles, ensuring alignment with the monthly mean values, and (ii) cumulative HDH consistency, whereby the characteristic day's total HDH closely matched the monthly average HDH. This selection methodology ensures that the chosen characteristic days effectively represent seasonal heating demand variations while maintaining high temporal accuracy. In this methodology, main factors such as the solar-air temperature ($T_{sa}(t)$), setpoint temperature ($T_{setpoint}$), and indoor air temperature (T_{indoor}) significantly influence heating demand. In the case of Muğla, the $T_{setpoint}$ was systematically varied between 16 °C and 26 °C in 2 °C increments, providing a detailed assessment of the region's climate across different seasons. This approach enables the optimization of heating systems by considering both seasonal fluctuations and Muğla's distinct climatic characteristics. Relevant parameters, including solar absorptivity, surface emissivity, and the total heat transfer coefficient, are provided in Table 1. Moreover, the analysis incorporated different fuel types along with their system efficiencies, unit costs, and emission factors for Muğla's energy consumption. This information, essential for evaluating the financial and environmental impacts of heating systems, is summarized in Table 2.

3. Results and discussion

This study investigates the pivotal role of free heating degree hours (HDH_{free}) in reducing the annual heating demand of buildings by maximizing the utilization of solar energy. Through the integration of the solar-air temperature (T_{sa}) concept, which accounts for solar radiation's contribution to heat gain, the methodology provides a highly accurate estimate of heating requirements and energy savings. By analyzing HDH_{free} under varying indoor setpoint temperatures and material properties such as absorptivity and emissivity, the study demonstrates how passive heating strategies can decrease dependence on mechanical systems. The significance of HDH_{free} values in free heating applications is evaluated in terms of energy savings and carbon footprint reduction across different fuel types, including electricity, natural gas, and fuel-oil. The methodology was validated using data from Muğla, Turkey, which was selected due to its distinct climatic conditions. For this region, hourly recorded data on ambient temperature and solar radiation were collected over a 31-year period and systematically incorporated into the methodology. The applicability of the T_{sa}-based free heating approach is strongly climate dependent; in regions with low winter solar radiation or persistent cloud cover, the T_{sa}–T_{amb} differential becomes small, which limits the effectiveness of free heating and necessitates recalibration of the model using local climatic datasets.

3.1. Climate characteristics and free heating potential

Fig. 2 presents a 31-year average temperature profile with maximum (T_{max}), minimum (T_{min}), and average ($T_{average}$) temperatures over time. The x-axis represents the days from January to December, while the left y-axis shows outside ambient temperature, and the right y-axis indicates solar radiation levels. Key elements include the indoor setpoint temperature ($T_{setpoint}$, red dashed line) and the solar radiation threshold ($I_{threshold}$, blue dashed line). Heating periods are identified when $T_{average}$ falls below $T_{setpoint}$, occurring from January to April and October to December. During summer (May to October), solar radiation levels exceeds $I_{threshold}$, reducing the need for active heating. Solar gain is more effective during this period, while winter conditions necessitate increased heating demand. Fig. 2 illustrates that heating demand arises when $T_{average}$ is below $T_{setpoint}$, particularly in colder months. However, when solar radiation surpasses $I_{threshold}$, the solar-air temperature (T_{sa}) can exceed the ambient temperature (T_{amb}), reducing the reliance on mechanical heating systems. This strategy highlights the potential for free heating during winter, as solar energy can elevate T_{sa} above $T_{setpoint}$ even when T_{amb} remains low. By incorporating solar radiation into the heating analysis, the building can sustain thermal comfort with reduced mechanical heating demand. The incorporation of T_{sa} has been expanded in this research to quantify free heating potential (HDH_{free}) and its economic/environmental implications. This approach provides a more precise evaluation of solar energy contributions to heating demand. Additionally, the figure emphasizes that passive heating can be effectively utilized when T_{sa} exceeds $T_{setpoint}$, particularly on sunny winter days. Using T_{sa} as an indicator of heating demand can lead to significant energy savings by optimizing solar gain.

Fig. 3 expands on this by showing temperature profiles for January, February, March, April, November, and December, comparing T_{max}, $T_{average}$, T_{min}, and T_{sa} throughout the day to assess free heating potential. Free heating occurs when T_{sa} surpasses $T_{setpoint}$, thereby reducing the demand of active heating. In January (Fig. 3a), T_{max} stays below 20 °C, and T_{sa} does not reach $T_{setpoint}$, indicating no free heating. In February (Fig. 3b), T_{sa} exceeds $T_{setpoint}$ between 09:30 and 16:30, peaking at 50 °C, providing approximately 7 h of free

Table 1
Parameters and technical characteristics for the methodology [55].

Parameters/technical characteristics	Values
Location	Muğla, Turkey
Sky temperature (T_{sky})	5, 7 and 9 °C
Solar absorptivity (α)	0.3, 0.5 and 0.7
Surface emissivity (ε)	0.35, 0.55 and 0.75
Total heat transfer coefficient (h_o)	1.8, 3.8 and 7.9 W/m^{2}K

Table 2
System efficiency, unit cost, and emission factors by fuel type [62].

Fuel type	System efficiency (%)	Unit cost ($/kWh)	Emission factor (kg CO_2/kWh)
Electricity	99	0.1059	0.588
Natural gas	93	0.0341	0.194
Fuel-oil	80	0.0651	0.268

Note: The UA value for external building walls in Muğla was assumed to be 0.6 W/K.

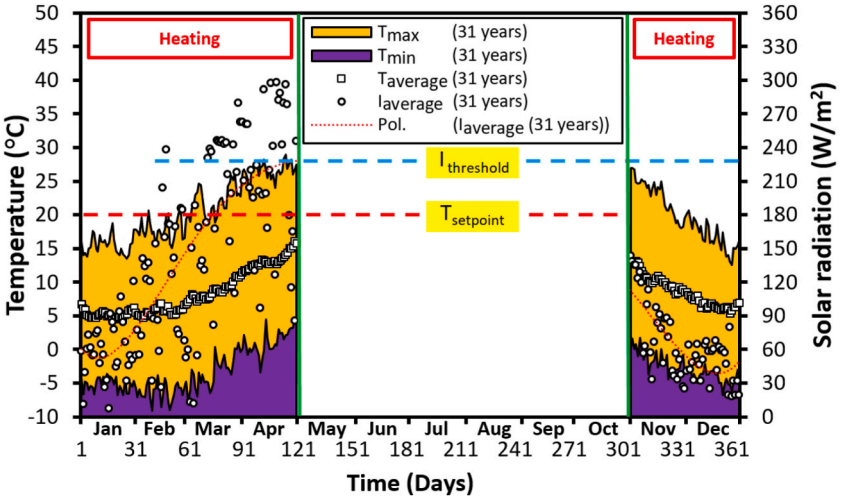

Fig. 2. 31-year average temperature profile showing maximum (T_{max}), minimum (T_{min}), and average ($T_{average}$) temperatures, with the indoor setpoint temperature ($T_{setpoint}$) and solar radiation threshold ($I_{threshold}$) for Muğla.

heating. March (Fig. 3c) exhibits a notable increase in T_{sa}, surpassing 35 °C for 9 h, indicating strong free heating potential. In April (Fig. 3d), T_{sa} exceeds 35 °C during midday, providing approximately 10 h of free heating, with a peak above 60 °C. November (Fig. 3e) offers limited free heating, with T_{sa} slightly surpassing $T_{setpoint}$ for 4 h. In December (Fig. 3f), T_{sa} remains below $T_{setpoint}$, similar to January, offering no free heating.

In Fig. 3b–e (February, March, April, and November), free heating occurs during midday (10:00–16:00), as T_{sa} exceeds $T_{setpoint}$. March and April exhibit the highest solar-air temperature peaks, exceeding 40 °C and 50 °C, respectively, demonstrating the greatest potential for passive heating. In contrast, January and December (Fig. 3a and f) show no significant free heating periods, with T_{sa} remaining below 20 °C. The increase in T_{max} in March and April, driven by higher solar radiation levels, extends the free heating window compared to earlier months. These figures indicate that February, March, April, and November provide substantial opportunities for free heating, particularly in March and April. Conversely, January and December offer minimal potential for free heating, emphasizing the importance of maximizing solar gains during transitional months to reduce heating energy demand.

3.2. *Effect of indoor setpoint temperature on heating demand*

Fig. 4 presents Heating Degree Hours (HDH) as a function of monthly and hourly variations for different setpoint temperatures. Fig. 4a compares monthly HDH values and the annual total across six setpoint temperatures. January and December show the highest HDH values, exceeding 12,000 °h at 26 °C. April and November have lower HDH, ranging between 8000 and 10,000 °h for higher setpoints and below 6000 °h for 16 °C. February and March display intermediate HDH values, from 8000 to 12,000 °h. On an annual scale, a setpoint temperature of 26 °C results in nearly 75,000 °h, whereas a 16 °C setpoint leads to approximately 40,000 °h, indicating that higher setpoints consistently increase heating demand, particularly in colder months. Fig. 4b illustrates hourly HDH for various setpoint temperatures. The highest HDH occurs at 26 °C, peaking at 4000 °h between 07:00 and 08:00 h, then decreasing to 2500 °h by 14:00–15:00 h. Lower setpoints, such as 16 °C, show a peak of 2500 °h in the early morning, dropping to 1000 °h in the afternoon. HDH values trend to be higher in the early morning (00:00 to 08:00 h) and lower between 12:00 and 16:00, before increasing again in the evening. Higher setpoint temperatures consistently add 1000–1500 °h more HDH across all hours compared to lower setpoints.

In Fig. 4a, higher setpoint temperatures (24 °C and 26 °C) result in substantial ly higher HDH values, particularly in January and December, where 26 °C exceeds 14,000 °h, whereas 16 °C reaches only 8000 °h. Fig. 4b shows a similar trend, with 26 °C peaking above 3500 °h in the early morning, compared to 2000 °h for 16 °C. Optimizing setpoint temperatures, particularly during peak heating hours and colder months, can lead to significant energy savings. Seasonal variations illustrated in Fig. 4a indicate that January and December have the highest heating demand, whereas April and November have lower HDH values, especially at setpoints like 16 °C. Daily patterns in Fig. 4b reveal that HDH peaks occur in the early morning and evening, with lower demand around midday

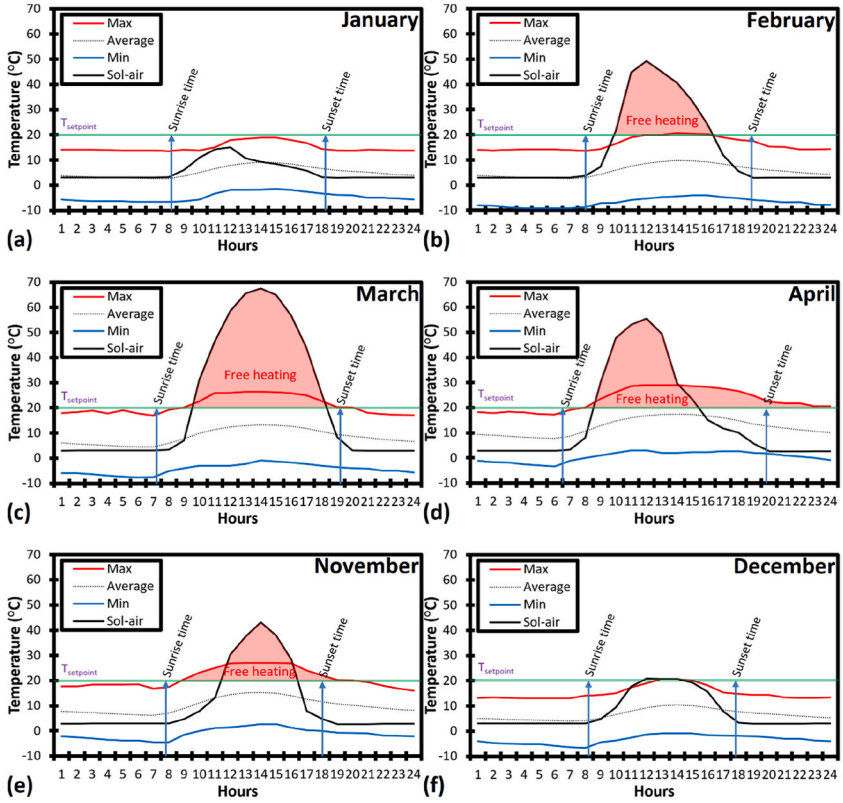

Fig. 3. Daily temperature profiles for various months; (a) January, (b) February, (c) March, (d) April, (e) November, and (f) December.

when outdoor temperatures rise. This suggests that heating systems could be dynamically adjusted to reduce midday heating demand, thereby enhancing overall efficiency. Overall, the data suggest that higher setpoint temperatures lead to greater heating demand. Lowering setpoints, especially during transitional months or midday hours, could reduce energy consumption by 25–40 %. A dynamic heating system that adjusts based on time of day and seasonal variations could optimize energy use, ensuring thermal comfort while minimizing energy demand. During colder months such as January and December, a higher setpoint could be maintained in the morning and lowered at midday. Conversely, in milder months like April and November, a lower setpoint could be sustained throughout the day, aligning with sustainable energy management practices.

Fig. 5 illustrates Free Heating Degree Hours (HDH_{free}) for different indoor setpoint temperatures (18 °C, 22 °C, 26 °C) and sky temperatures (5 °C, 7 °C, 9 °C), showing both (a) monthly and (b) hourly variations. Fig. 5a compares HDH_{free} across months (January, February, March, April, November, December) and the annual total. March consistently shows the highest HDH_{free}, exceeding 20,000 °h for all combinations. February and April also show high values, ranging from 12,000 to 18,000 °h. January and December exhibit moderate values (6000 to 12,000 °h), while November has the lowest, below 8000 °h. Lower sky temperatures (5 °C) consistently result in higher HDH_{free}, and higher setpoints (26 °C) increase free heating potential. Annual totals range from 40,000 to 55,000 °h, indicating that March has the greatest free heating potential, with February and April also offering significant opportunities. Lower sky temperatures and higher setpoints further enhance this potential, suggesting optimization of these parameters can reduce heating demand. Fig. 5b shows hourly HDH_{free} variations over 24 h. Peaks occur between 10:00 and 14:00 h, with the highest values (around 9500 °h) for the 5 °C-18 °C combination and the lowest (around 7000 °h) for the 9 °C-26 °C combination. Lower sky temperatures and setpoints consistently yield higher HDH_{free} across all hours. A difference of approximately 2500 °h is observed between lower (18 °C) and higher (26 °C) setpoints at peak hours. This indicates that free heating is most effective during midday, especially with lower sky and setpoint temperatures.

In both Fig. 5a and b, lower setpoints (18 °C) and sky temperatures (5 °C) consistently provide higher HDH_{free}. March emerges as the optimal month for free heating, offering up to 20,000 °h. Adaptive control strategies that adjust setpoints seasonally can maximize energy savings. The daily pattern in Fig. 4b highlights the midday peak, suggesting that heating systems should capitalize on peak solar hours for enhanced free heating efficiency. The results of this study demonstrate that incorporating T_{sa} into heating demand calculations significantly enhances the accuracy of heating load estimation. Comparisons with previous studies indicate that traditional HDH models tend to underestimate passive heating potential due to their reliance on ambient temperature alone. For instance, Ghiaus [45] and De Rosa et al. [46] incorporated solar irradiation into degree-hour calculations, yet their models primarily relied on static coefficients rather than dynamic environmental parameters. In contrast, this study dynamically integrates solar radiation and radiative heat loss effects, resulting in a more precise estimation of HDH_{free}. Furthermore, the results suggest that optimizing setpoint

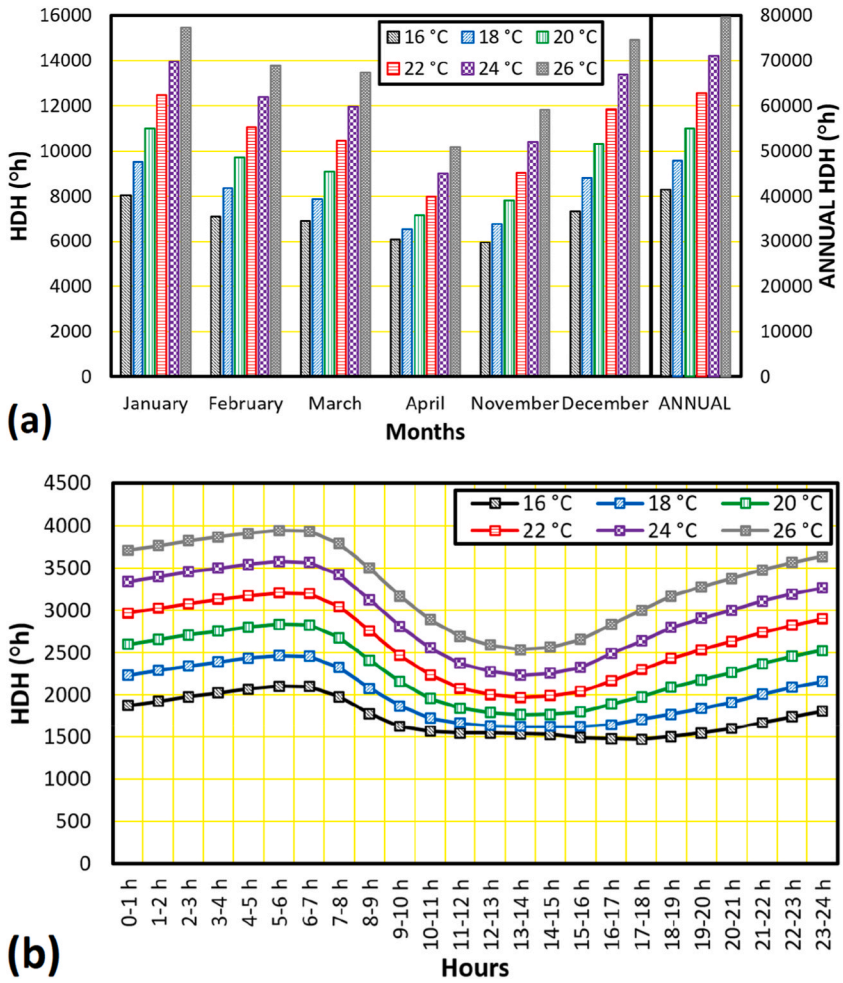

Fig. 4. Comparison of HDH across different months (a) and hours of the day (b) for various setpoint temperatures.

temperatures, selecting high solar absorptivity materials ($\alpha \geq 0.7$), and minimizing surface emissivity ($\varepsilon \leq 0.35$) can significantly enhance passive heating efficiency. These results align with previous research on passive heating strategies (e.g., Harvey [47] and Zhang et al. [49]), but this study uniquely quantifies the direct contribution of solar-air temperature to heating demand reduction, thus bridging the gap between theoretical modeling and practical implementation in energy-efficient building design. Annual HDH_{free} values, ranging from 40,000 to 55,000 °h, demonstrate the potential for significant energy savings, with reductions of 25–30 % in energy use achievable through dynamic setpoint adjustments. This would decrease reliance on mechanical heating and result in substantial economic benefits, particularly in colder climates. Since heating demand calculations in this study were conducted on an hourly basis, it is crucial to evaluate the interplay between free heating potential and thermal inertia effects within a time-sensitive context. The results indicate that free heating is most effective during peak solar hours (10:00–16:00), significantly reducing mechanical heating demand during the day. Conversely, thermal inertia plays a vital role in minimizing temperature fluctuations and mitigating heating demand during nighttime hours by storing solar energy absorbed during the day. These results highlight the necessity of adopting an integrated approach that optimally combines free heating potential and thermal mass properties to enhance energy efficiency and reduce heating loads. This qualitative interpretation does not imply that thermal inertia is explicitly modeled within the HDH_{free} equations; rather, thermal mass is discussed to contextualize the physical response of envelope materials.

3.3. *Effect of building material properties on free heating*

Fig. 6 illustrates the relationship between setpoint temperatures and solar absorptivity on HDH_{free}, highlighting the impact of these factors on passive heating potential across different months and daily cycles. Fig. 6a shows the variation in HDH_{free} based on setpoint temperatures (indoor) and solar absorptivity across different months and the annual total. The highest annual HDH_{free} is at 18 °C with 0.7 absorptivity, exceeding 82,000 °h, while the lowest, at 26 °C with 0.3 absorptivity, is around 19,418 °h. March consistently has the highest HDH_{free}, while December shows the lowest, reflecting less effective free heating in winter. Increasing solar absorptivity from 0.3 to 0.7 significantly boosts HDH_{free} across all months and setpoints, with annual values rising from 27,712 to 82,206 °h at 18 °C.

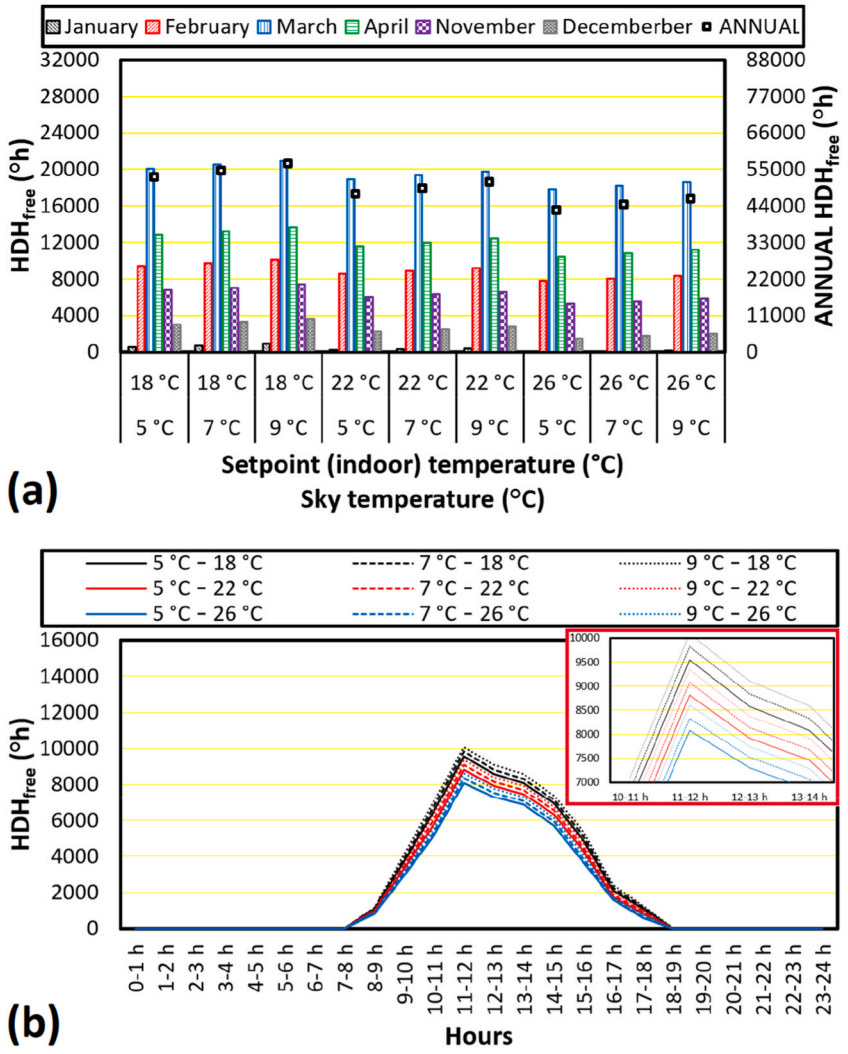

Fig. 5. Free Heating Degree Hours (HDH_{free}) for various indoor setpoint and sky temperatures shown across different (a) months and (b) hours of the day.

Lower setpoints and higher absorptivity maximize free heating, especially in transitional months like March. December and January show the least potential, indicating a need for supplemental heating during colder months. Fig. 6b presents the hourly variation of HDH_{free} for different setpoints and solar absorptivity throughout the day. The HDH_{free} peaks between 10:00 and 14:00, with a maximum of around 14,000 °h at 18 °C and 0.7 absorptivity, demonstrating optimal free heating during midday when solar radiation is strongest. Increasing solar absorptivity from 0.3 to 0.7 raises HDH_{free} across all setpoints. At 18 °C, the peak HDH_{free} increases from 10,000 to over 14,000 °h, a 40 % improvement. Higher setpoints reduce HDH_{free}, with 26 °C showing around 10,000 °h at the same absorptivity. Lower setpoints and higher absorptivity significantly enhance free heating, particularly during midday hours. In summary, optimizing solar absorptivity and setpoint temperatures is essential for maximizing free heating potential. Midday solar gains are particularly effective in months like March. Prioritizing lower setpoints and higher absorptivity materials can lead to substantial energy savings, reducing the need for mechanical heating and lowering carbon emissions. These findings, however, apply exclusively to heating-dominated periods in which $T_{amb} < T_{setpoint}$, and the HDH_{free} framework was not extended to summer conditions. Consequently, the potential cooling penalties associated with high-absorptivity façades remain outside the present scope. Integrating the HDH_{free} formulation with cooling-degree-hour and overheating indicators would provide a more holistic, year-round performance evaluation, especially for Mediterranean climates where summer cooling demand is significant.

Fig. 7 illustrates the effect of setpoint temperatures and surface emissivity on HD_{Hfree}, showing how optimizing these parameters can enhance passive heating efficiency across different months and times of day. Fig. 7a shows the variation in HDH_{free} based on setpoint temperatures and surface emissivity, with data presented monthly and annually. The highest annual HDH_{free} is 56,446 °h at 18 °C and 0.35 emissivity, demonstrating that lower emissivity and lower setpoints maximize free heating. The lowest HDH_{free}, 42,731 °h, occurs at 26 °C and 0.75 emissivity, indicating that higher emissivity and setpoints reduce passive heating potential. March

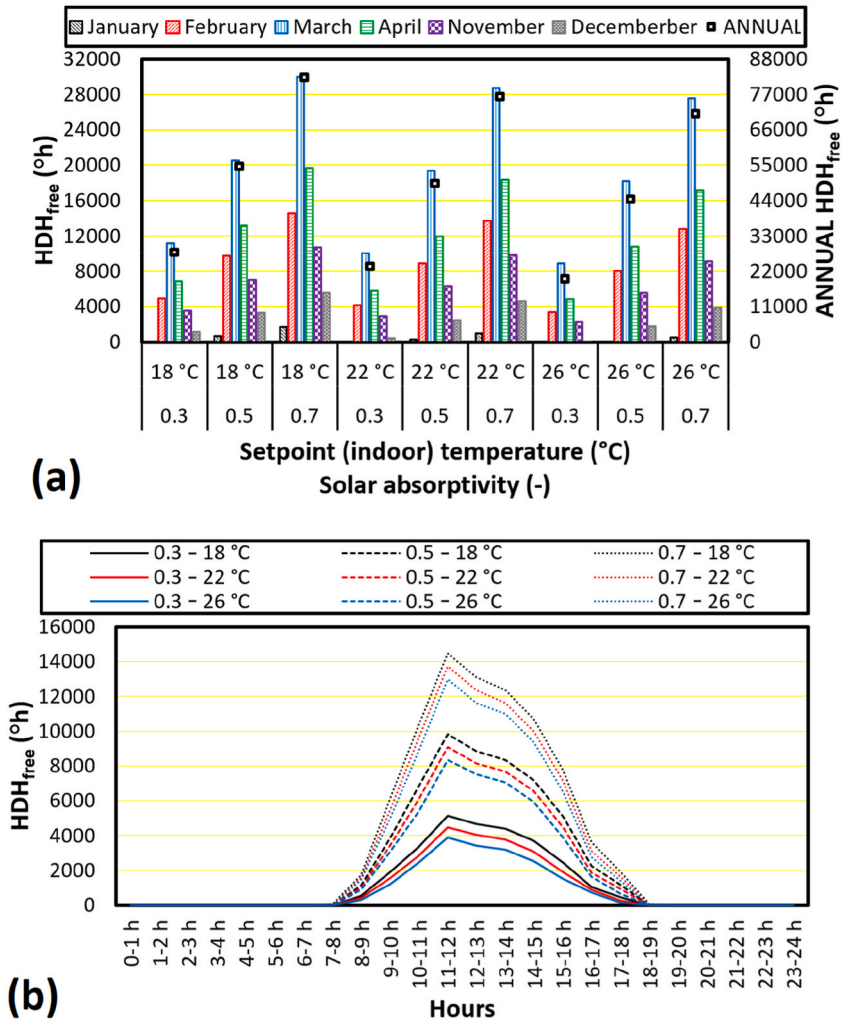

Fig. 6. Variation of HDH_{free} as a function of setpoint temperature and solar absorptivity, showing (a) monthly, annual, and (b) hourly distributions.

consistently provides the highest HDH_{free} across all settings, peaking at 20,927 °h at 18 °C and 0.35 emissivity, while December contributes the least, with only 3419 °h at the same settings. Lower emissivity materials retain heat more effectively, resulting in higher HDH_{free} across all setpoints. Increasing emissivity to 0.75 reduces HDH_{free} by 6.7 % at 18 °C. Using materials with low emissivity and maintaining lower setpoints significantly improves free heating, particularly in high solar radiation months like March.

Fig. 7b illustrates the hourly variation of HDH_{free} for different setpoint temperatures and surface emissivity values, with peaks occurring between 10:00 and 14:00. At 18 °C and 0.35 emissivity, the peak HDH_{free} reaches 10,053 °h between 11:00 and 12:00, indicating maximum heat retention. At 26 °C and 0.75 emissivity, the peak HDH_{free} drops to 8100 °h, reflecting reduced passive heating potential with higher setpoints and emissivity. Lower emissivity values consistently lead to higher HDH_{free} across all setpoints. For example, at 18 °C, HDH_{free} decreases by 4.7 % from 10,053 °h at 0.35 emissivity to 9582 °h at 0.75 emissivity. Higher setpoints further reduce HDH_{free}, as seen at 0.35 emissivity, where HDH_{free} drops from 10,053 °h at 18 °C to 8577 °h at 26 °C.

Fig. 7 highlights the importance of optimizing setpoint temperatures and surface emissivity for passive heating efficiency. Fig. 7a shows that lower emissivity (0.35) consistently results in higher annual HDH_{free}, with a 6.7 % reduction observed when emissivity increases from 0.35 to 0.75 at 18 °C. Similarly, Fig. 7b demonstrates that lower emissivity enhances passive heating during peak solar hours, with peak HDH_{free} at 18 °C reaching 10,053 °h compared to 8100 °h at 26 °C. Setpoint temperature also plays a critical role, with annual HDH_{free} decreasing by 24.3 % from 18 °C to 26 °C. Overall, optimizing emissivity and setpoint temperatures significantly increases HDH_{free}, particularly during midday and in months like March. Lowering emissivity and setpoints enhances passive heating efficiency, reduces energy consumption, and improves building sustainability.

3.4. Impact of heat transfer coefficient on free heating efficiency

Fig. 8 illustrates the impact of setpoint temperatures and heat transfer coefficients on HDH_{free}, highlighting how optimizing these

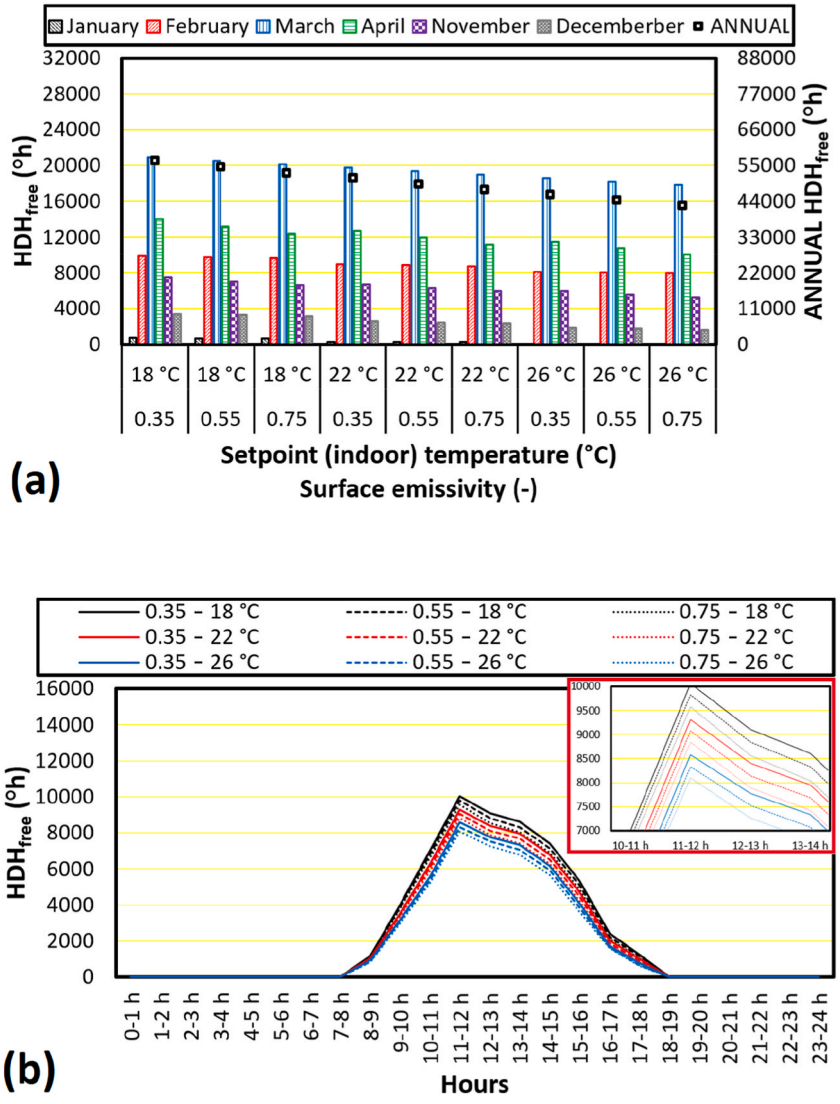

Fig. 7. Variation of HDH_{free} as a function of setpoint temperature and surface emissivity, showing (a) monthly, annual, and (b) hourly distributions.

parameters can enhance passive heating efficiency throughout the year and during peak solar hours. Fig. 8a shows the annual and monthly variation of HDH_{free} based on setpoint temperatures and heat transfer coefficients (h_o), ranging from 1.8 W/m^2K to 7.9 W/m^2K. The highest annual HDH_{free} occurs at 18 °C with 1.8 W/m^2K, reaching 126,311 °h, indicating that lower heat transfer coefficients maximize heat retention and free heating potential. In contrast, the lowest HDH_{free}, 14,683 °h, is seen at 26 °C and 7.9 W/m^2K, reflecting reduced passive heating efficiency with higher ho values and setpoint temperatures. Monthly, March shows the highest HDH_{free}, particularly at lower ho values, with 45,575 °h at 18 °C and 1.8 W/m^2K. December has the lowest HDH_{free}, with just 10 °h at 26 °C and 7.9 W/m^2K, indicating minimal passive heating in colder months. As h_o increases, HDH_{free} decreases significantly across all setpoints, dropping by 82.2 % from 126,311 °h at 1.8 W/m^2K to 22,530 °h at 7.9 W/m^2K at 18 °C. Lower setpoints (18 °C) consistently show higher HDH_{free} for all ho values, with a 9.9 % reduction from 18 °C to 26 °C at 1.8 W/m^2K. Optimizing both heat transfer coefficients and setpoints is essential for maximizing free heating, especially during months like March, where solar gains are high.

Fig. 8b shows hourly variation of HDH_{free} based on setpoints and heat transfer coefficients. The peak HDH_{free} occurs between 10:00 and 14:00, with the highest value of 22,045 °h at 18 °C and 1.8 W/m^2K around noon. The lowest peak, 2994 °h, is observed at 26 °C and 7.9 W/m^2K, demonstrating how higher setpoints and heat transfer coefficients reduce free heating potential. At 18 °C, HDH_{free} decreases by 81.2 % from 22,045 °h at 1.8 W/m^2K to 4143 °h at 7.9 W/m^2K. Lower setpoints provide significantly higher HDH_{free} across all ho values, with HDH_{free} dropping from 22,045 °h at 18 °C to 14,503 °h at 26 °C. The midday peak between 10:00 and 14:00 aligns with maximum solar radiation, with lower heat transfer coefficients improving heat retention during these hours, optimizing passive heating efficiency.

Fig. 8 highlights the importance of setpoint temperatures and heat transfer coefficients in optimizing passive heating. Fig. 8a shows

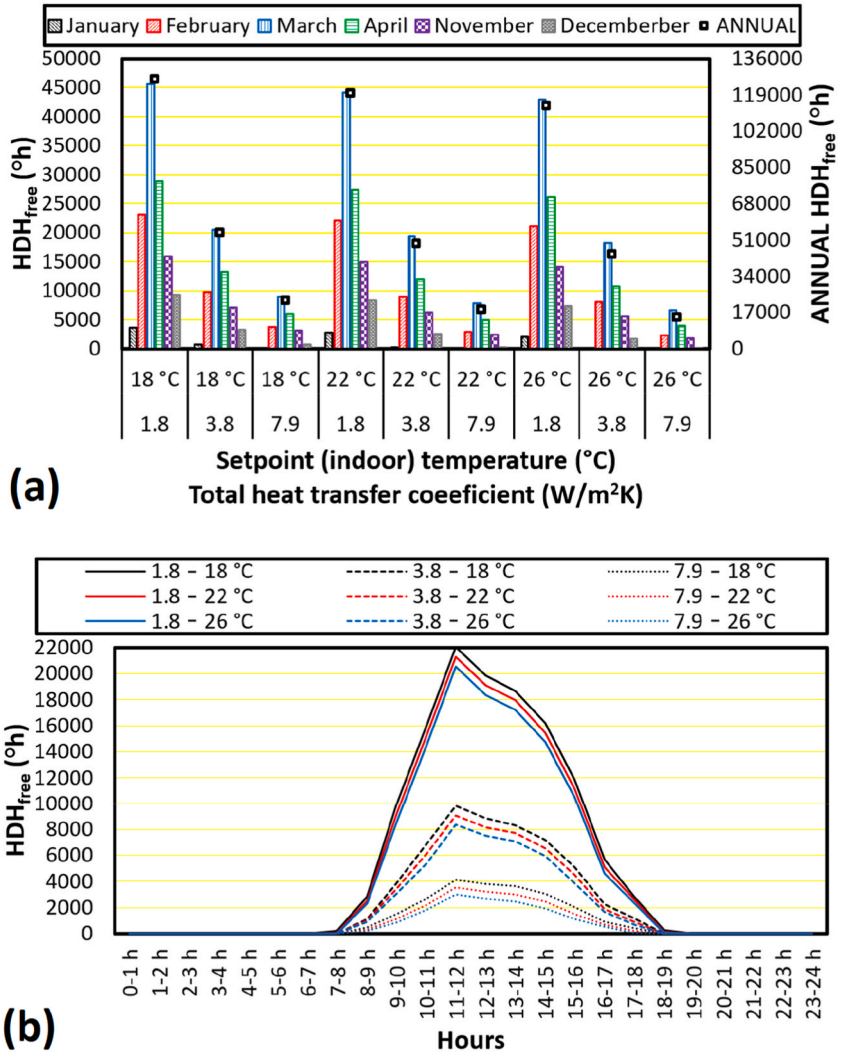

Fig. 8. Variation of HDH_{free} as a function of setpoint temperature and heat transfer coefficient, showing (a) monthly, annual, and (b) hourly distributions.

that lower ho values (1.8 W/m^{2}K) combined with lower setpoints (18 °C) yield the highest annual HDH_{free}, while higher ho values reduce free heating by up to 82.2 %. Fig. 8b reveals that midday solar radiation is most effectively utilized with lower ho and setpoint values, maximizing HDH_{free}. Optimizing insulation and setpoint temperatures enhances passive heating efficiency, reduces energy consumption, and improves sustainability, particularly during peak solar hours and in months like March.

Fig. 9 demonstrates the effect of different free heating scenarios, including combinations of sky temperature (T_{sky}), absorptivity (α), emissivity (ε), heat transfer coefficient (h_o), and setpoint temperatures (from 16 °C to 26 °C), on energy savings. The figure effectively illustrates how material properties and environmental factors influence the efficiency of passive heating systems. The h_o plays a significant role, with lower values (1.8 W/m^{2}K) leading to the highest energy savings. For example, in the case of $T_{sky} = 7$ °C, $\alpha = 0.5$, and $\varepsilon = 0.55$, energy savings reach 313 % at a 16 °C setpoint. When h_o increases to 7.9 W/m^{2}K, savings drop dramatically to 60 %, reflecting an 80.8 % reduction. This shows that optimizing insulation by reducing heat transfer is critical for maximizing passive heating efficiency. Setpoint temperature also strongly affects energy savings. Lower setpoints consistently result in greater savings. For instance, in the scenario with $T_{sky} = 7$ °C, $\alpha = 0.5$, $\varepsilon = 0.55$, and $h_o = 1.8$ W/m^{2}K, savings decrease from 313 % at 16 °C to 143 % at 26 °C—a 54.3 % drop. This highlights the importance of maintaining lower indoor temperatures to fully benefit from free heating. Absorptivity (α) and emissivity (ε) also influence the system's performance. Higher absorptivity materials ($\alpha = 0.7$) increase energy savings, as they absorb more solar energy. For instance, under the same conditions, increasing α from 0.3 to 0.7 raises energy savings from 73 % to 206 % at a 16 °C setpoint, an increase of 182 %. Lower emissivity ($\varepsilon = 0.35$) further enhances performance by reducing radiative heat losses, increasing savings from 134 % to 143 % when compared to higher emissivity materials ($\varepsilon = 0.75$). Although T_{sky} has a lesser impact than h_o or setpoint temperatures, higher T_{sky} values do result in modest energy savings improvements. For example, increasing T_{sky} from 5 °C to 9 °C under constant conditions only boosts energy savings from 133 % to 144 %, indicating that while it

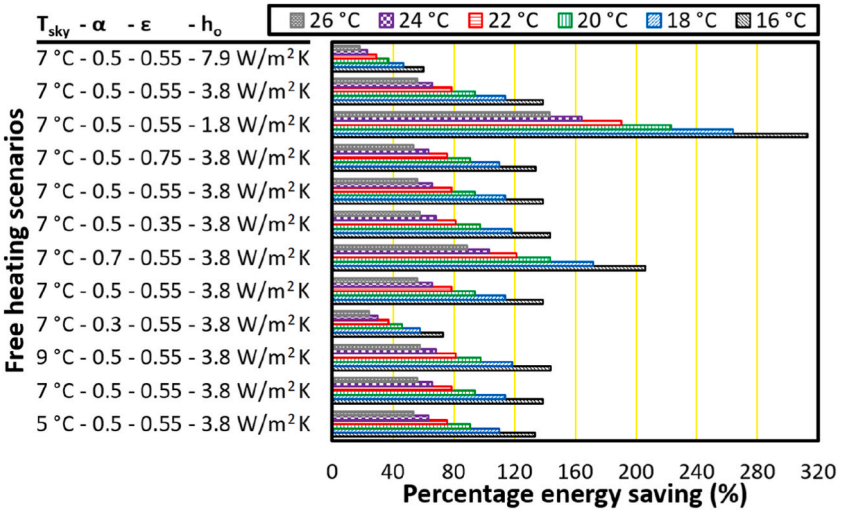

Fig. 9. Variation of the percentage energy savings across various free heating scenarios.

plays a role, the focus should remain on optimizing material properties and insulation. Maximizing energy savings in passive heating systems requires low heat transfer coefficients, moderate to high absorptivity, and low emissivity. Maintaining lower setpoint temperatures significantly extends the potential for free heating, especially in colder climates and during low solar radiation periods. These findings emphasize the importance of careful material selection and design to optimize heating efficiency and reduce energy consumption.

Figs. 5–9 reveal critical insights into optimizing free heating potential and energy efficiency across various scenarios involving sky temperature, solar absorptivity, emissivity, heat transfer coefficients, and indoor setpoint temperatures. The data consistently show that lowering the indoor setpoint temperature (particularly to 18 °C) and minimizing heat transfer coefficients (h_o = 1.8 W/m^{2}K) significantly increase the HDH_{free}, particularly during high solar radiation periods, such as midday (10:00–14:00).

3.5. *Economic and environmental benefits of free heating*

Fig. 10 illustrates energy cost savings in free heating scenarios based on sky temperature, solar absorptivity, emissivity, and heat transfer coefficient for electricity, natural gas, and fuel-oil as heating fuels. Fig. 10a shows energy savings for electricity-based heating, comparing indoor temperatures of 18 °C, 22 °C, and 26 °C. The highest savings are achieved at 18 °C with h_o = 1.8 W/m^{2}K, T_{sky} = 7 °C, α = 0.5, and ε = 0.55, yielding 8107 $/m^2/year. As the indoor temperature increases to 26 °C, savings drop by 10 %, to 7297 $/m^2/year. The heat transfer coefficient has the most significant impact on savings; for example, increasing ho from 1.8 to 7.9 W/m^{2}K reduces savings by 82 %, from 8107 to 1446 $/m^2/year. This demonstrates the importance of optimizing heat transfer and emissivity, especially at lower indoor temperatures, to maximize cost savings in electricity-based systems.

Fig. 10b presents energy savings for natural gas heating. The highest savings occur at 18 °C and h_o = 1.8 W/m^{2}K, reaching 2779 $/m^2/year. As the temperature increases to 26 °C, savings decrease by 10 %, to 2501 $/m^2/year. Higher heat transfer coefficients significantly reduce savings; for instance, increasing ho from 1.8 to 7.9 W/m^{2}K lowers savings by 82 %, from 2779 to 496 $/m^2/year. Emissivity and solar absorptivity have a smaller impact, but lower emissivity (0.35) offers marginally better performance. Minimizing heat transfer coefficients remains the key factor in maximizing savings with natural gas. Fig. 10c shows energy savings for fuel-oil heating. The highest savings, 6167 $/m^2/year, are seen at 18 °C and h_o = 1.8 W/m^{2}K. As the indoor temperature increases to 26 °C, savings reduce to 5551 $/m^2/year, a 10 % decrease. When ho is increased to 7.9 W/m^{2}K, savings drop by 82 %, from 6167 to 1100 $/m^2/year. Similar to the other fuels, optimizing ho is the most effective way to maximize savings. Emissivity and absorptivity adjustments provide smaller improvements.

Fig. 10 shows consistent trends across all heating fuels: lower indoor temperatures (18 °C) and lower heat transfer coefficients (h_o = 1.8 W/m^{2}K) lead to the highest savings. Electricity offers the greatest potential savings, reaching 8107 $/m^2/year, followed by fuel-oil (6167 $/m^2/year) and natural gas (2779 $/m^2/year). Reducing ho significantly increases savings for all fuels, with electricity seeing an 82 % increase and natural gas showing a 450 % increase. Changes in emissivity (ε) and solar absorptivity (α) have a smaller effect, but still provide modest improvements when ho is optimized. Overall, minimizing ho and maintaining lower indoor temperatures are crucial for maximizing energy cost savings, especially in electricity-based systems.

Fig. 11 illustrates carbon footprint reductions across various free heating scenarios using electricity, natural gas, and fuel-oil as heating fuels. Fig. 11a shows carbon reductions when electricity is the primary energy source. The highest reduction, 45 tons CO_2/m^{2}year, is achieved at 18 °C and h_o = 1.8 W/m^{2}K, while at 26 °C, this drops by 9 %–41 tons CO_2/m^{2}year. With a higher heat transfer coefficient (7.9 W/m^{2}K), the reduction is minimal, ranging from 8 tons CO_2/m^{2}year at 18 °C to 5 tons CO_2/m^{2}year at 26 °C. Lowering ho from 7.9 to 1.8 W/m^{2}K provides the most significant carbon savings, particularly at lower temperatures. While variations in solar

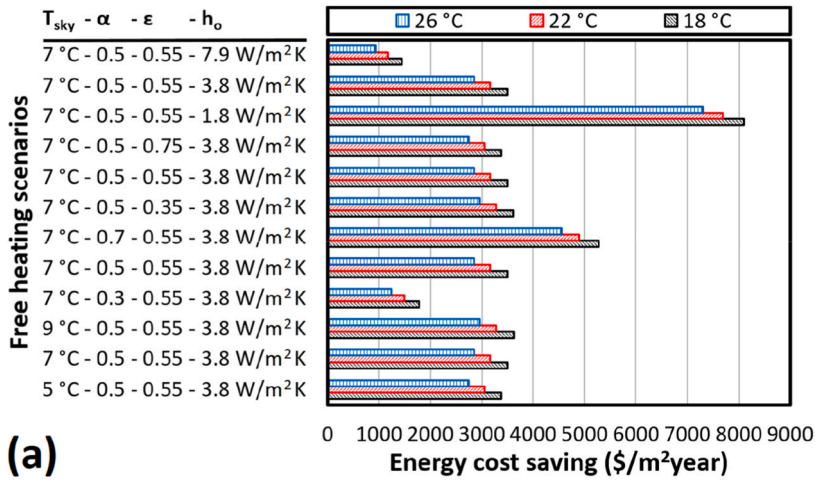

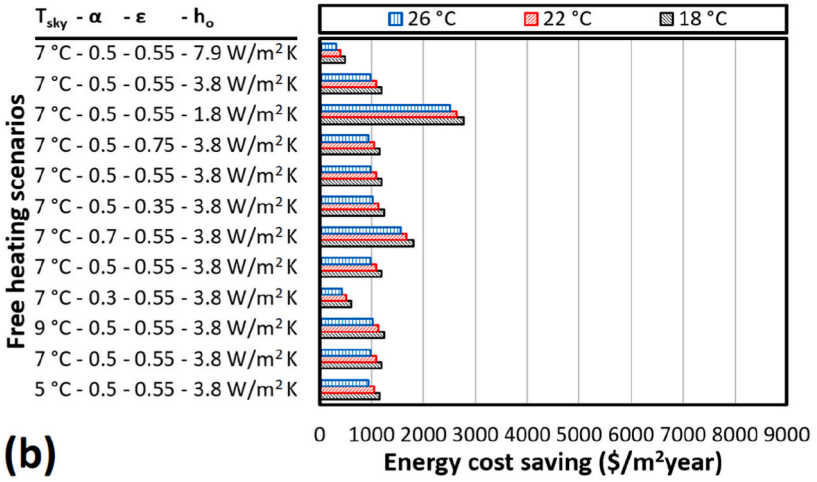

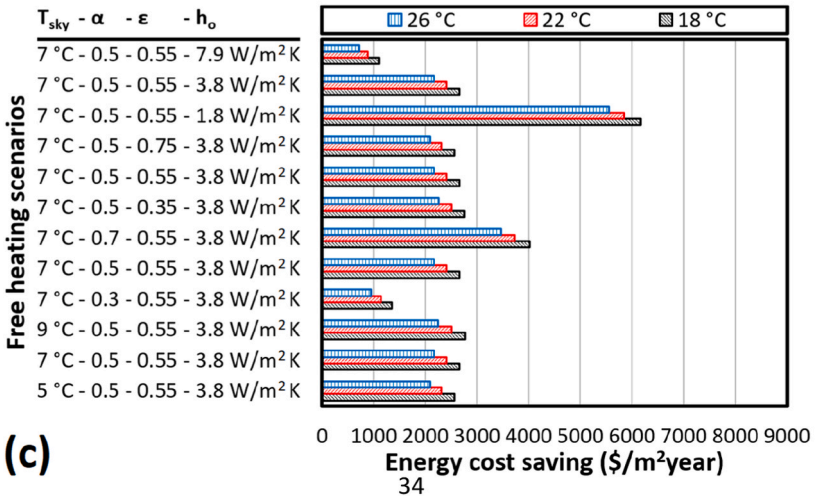

Fig. 10. Energy cost savings across various free heating scenarios for (a) electricity, (b) natural gas, and (c) fuel-oil.

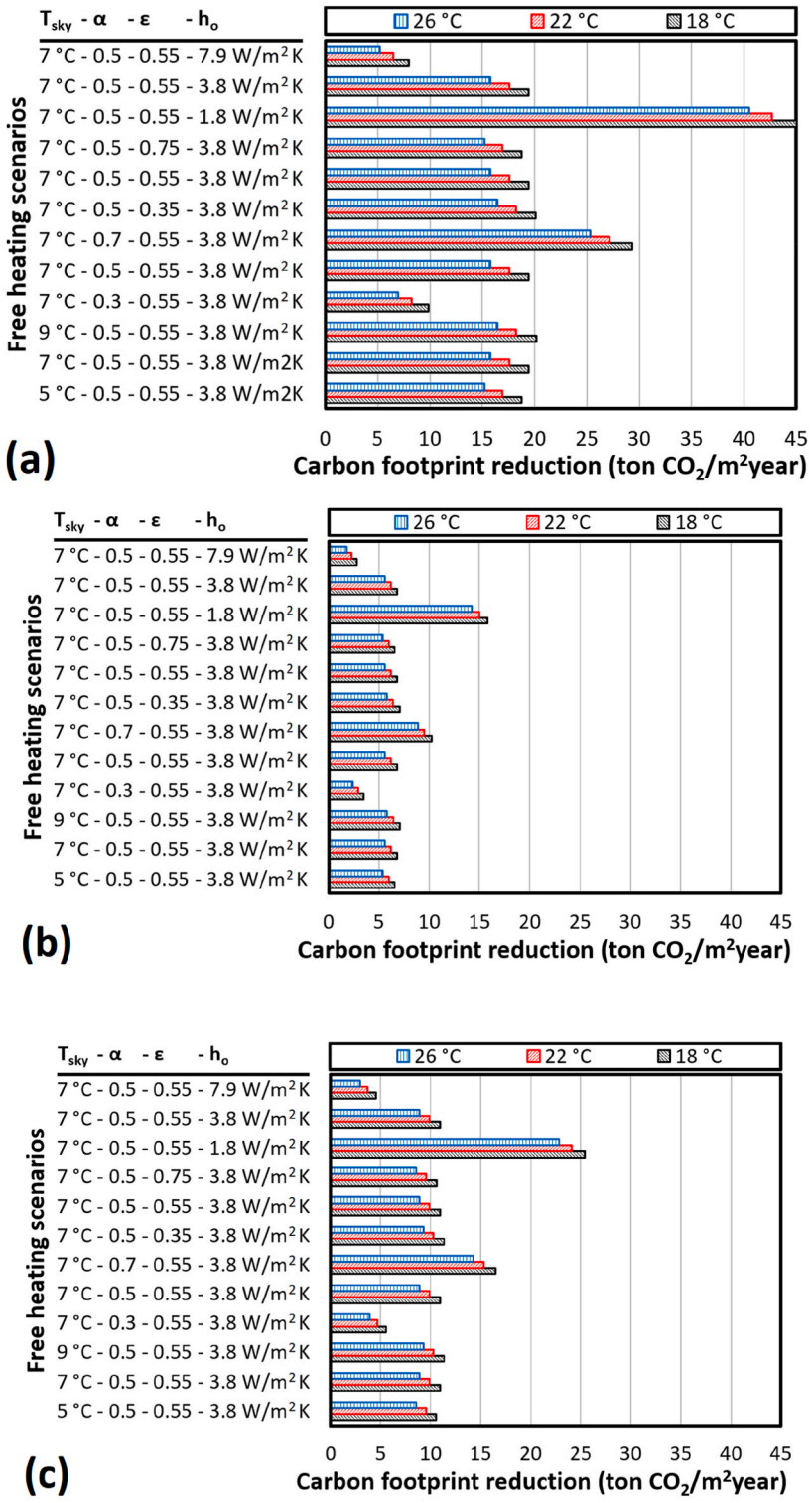

37

Fig. 11. Carbon footprint reduction across different fuel types; (a) electricity, (b) natural gas, and (c) fuel-oil, under varying free heating scenarios.

absorptivity (α) and emissivity (ε) have a smaller effect, optimizing ho has the greatest impact on reducing carbon footprints in electricity-based systems.

Fig. 11b presents carbon reductions for natural gas heating. The highest reduction is 16 tons CO_2/m^2year at 18 °C and $h_o = 1.8$ W/m^2K, dropping to 14 tons CO_2/m^2year at 26 °C, a 12.5 % decrease. With a high h_o (7.9 W/m^2K), reductions fall to 3 tons CO_2/m^2year at 18 °C and 2 tons CO_2/m^2/year at 26 °C. Reducing ho has the greatest impact on carbon reduction, while variations in α and ε have a more modest effect. Optimizing heat transfer coefficients is key to maximizing carbon savings with natural gas. Fig. 11c shows carbon reductions for fuel-oil heating. The highest reduction is 25 tons CO_2/m^2year at 18 °C and $h_o = 1.8$ W/m^2K, decreasing to 23 tons CO_2/m^2year at 26 °C, an 8 % drop. With $h_o = 7.9$ W/m^2K, reductions drop to 5 tons CO_2/m^2year at 18 °C and 3 tons CO_2/m^2year at 26 °C. As with electricity and natural gas, reducing ho offers the most significant carbon savings. Changes in α and ε have less impact, but optimizing ho remains critical for maximizing carbon reduction in fuel-oil systems.

Across all fuel types, carbon reductions are highest at lower indoor temperatures (18 °C), with electricity showing the greatest reduction at 45 tons CO_2/m^2year, followed by fuel-oil at 25 tons CO_2/m^2/year, and natural gas at 16 tons CO_2/m^2year. As indoor temperature increases to 26 °C, carbon savings decrease by 9 % for electricity, 12.5 % for natural gas, and 8 % for fuel-oil. Lowering ho from 7.9 to 1.8 W/m^2K significantly increases carbon savings for all fuels, with electricity seeing an 82 % increase. While changes in α and ε offer moderate improvements, optimizing insulation and heat transfer remains the most effective strategy for reducing carbon footprints in free heating systems.

3.6. Discussion

The results of this study underscore the significant role of free heating potential (HDH_{free}) in optimizing heating demand and energy efficiency by incorporating the solar-air temperature (T_{sa}) concept. The results indicate that key factors such as indoor setpoint temperature, material properties (absorptivity and emissivity), and heat transfer coefficient (h_o) directly influence the effectiveness of passive heating strategies. Across various scenarios, a lower setpoint temperature (particularly around 18 °C) and minimizing the heat transfer coefficient (1.8 W/m^2K) consistently led to a higher HDH_{free} and reduced reliance on mechanical heating systems. These findings suggest that dynamic adjustments to setpoint temperatures, particularly in transitional months, can significantly contribute to energy savings while maintaining thermal comfort.

The impact of building material properties on free heating efficiency is also evident. High solar absorptivity (α) enhances heat gain, especially during peak solar radiation hours, whereas low surface emissivity (ε) minimizes radiative heat loss, effectively increasing heat retention within the building envelope. This suggests that selecting materials with high absorptivity ($\alpha \geq 0.7$) and low emissivity ($\varepsilon \leq 0.35$) can maximize the benefits of free heating, particularly in climates with significant seasonal solar variation. Furthermore, optimizing insulation performance through lower heat transfer coefficients reduces energy demand by minimizing thermal losses. The findings reinforce the idea that an integrated approach, combining solar-air temperature utilization, material selection, and setpoint optimization, can drastically enhance passive heating efficiency.

From an economic and environmental perspective, the energy cost savings and carbon footprint reduction achieved through free heating are substantial. The results indicate that electricity-based heating systems offer the highest cost savings, with reductions up to 8107 \$/m^2/year under optimal conditions. Natural gas and fuel-oil systems also exhibit significant savings, but the economic benefits are more pronounced when heat transfer coefficients are minimized and setpoint temperatures are adjusted dynamically. Additionally, the carbon footprint analysis demonstrates that free heating strategies can lead to significant CO_2 reductions, particularly in electricity-based systems, where savings of up to 45 tons CO_2/m^2/year were observed. These results emphasize the necessity of integrating free heating strategies into sustainable building design, reducing dependency on fossil fuels while promoting environmentally friendly heating solutions.

Despite these promising outcomes, the methodology has certain limitations. The study's results are highly dependent on accurate solar radiation and ambient temperature data, which can vary spatially and temporally. This dependence introduces uncertainties in the estimation of HDH_{free}, particularly in locations with fluctuating or unpredictable weather conditions. Additionally, while the solar-air temperature approach provides a precise estimation of free heating potential, it does not fully account for external factors such as building shading, orientation, and urban heat island effects, which can significantly influence solar gains and overall heating demand. In conclusion, this study highlights the importance of optimizing setpoint temperatures, material properties, and heat transfer coefficients to enhance free heating potential. The results confirm that passive heating strategies can significantly reduce mechanical heating demand, lower energy costs, and mitigate carbon emissions.

4. Conclusion

This study presents a novel methodology for optimizing heating demand and energy savings by incorporating the solar-air temperature (T_{sa}) concept into the calculation of heating degree hours (HDH) and free heating degree hours (HDH_{free}). The primary innovation of this work lies in its integration of solar radiation's influence on building heating demand, allowing for a more precise estimation of free heating potential. By considering the solar-air temperature instead of ambient temperature, the methodology accounts for both solar gain and radiative heat loss, providing a significant improvement over conventional heating demand calculations. The scientific niche this article addresses is the enhancement of passive heating systems in building energy management, particularly in climates with significant seasonal variations. It bridges the gap between conventional heating degree-hour calculations and the practical implementation of solar-energy-based heating solutions, offering a comprehensive framework for reducing reliance on mechanical systems. Thus, this study has outlined the following main conclusions:

- Lowering indoor setpoint temperatures, particularly to 18 °C, led to a 25–40 % reduction in annual heating demand, maximizing free heating efficiency during peak solar hours (10:00–14:00). This demonstrates that setpoint optimization alone can significantly reduce energy consumption, especially in colder months like January and December.
- Reducing the heat transfer coefficient (h_o) from 7.9 W/m^{2}K to 1.8 W/m^{2}K resulted in an 82 % increase in free heating potential, with a peak HDH_{free} of 126,311 °h. Optimizing ho is crucial for maximizing energy savings, especially in high solar gain months such as March.
- Increasing solar absorptivity from 0.3 to 0.7 raised HDH_{free} by 40 %, contributing to energy savings of up to 313 % at a 16 °C setpoint. Materials with higher absorptivity can enhance solar gain and passive heating efficiency, particularly during midday.
- Lowering surface emissivity from 0.75 to 0.35 resulted in a 6.7 % increase in annual HDH_{free} and a 40 % improvement in midday free heating efficiency. Lower emissivity materials enhance heat retention, reducing the reliance on mechanical systems during winter months.
- The highest energy savings were achieved in electricity-based heating systems, with a maximum of 8107 $/m^2/year at a setpoint of 18 °C and $h_o = 1.8$ W/m^{2}K. Optimizing setpoint temperatures and heat transfer coefficients can reduce heating costs by 25–30 %, particularly for electricity and fuel-oil systems.
- Lowering h_o from 7.9 to 1.8 W/m^{2}K reduced carbon emissions by up to 82 %, with the highest reduction of 45 tons CO_2/m^{2}year seen in electricity-based systems. Effective insulation and lower setpoints are essential for maximizing environmental benefits.
- The combination of free heating and thermal inertia plays a critical role in energy efficiency. Free heating significantly reduces daytime heating demand by utilizing solar gains, whereas thermal inertia enhances nighttime thermal comfort by stabilizing indoor temperatures. An optimal design strategy should incorporate both high solar absorptivity materials for maximizing free heating and high thermal inertia materials for prolonged heat retention, ensuring a well-balanced and energy-efficient heating system.
- March consistently provided the highest free heating potential, with HDH_{free} exceeding 20,000 °h across all scenarios. Transitional months like March and April offer substantial opportunities for reducing heating demand through passive solar gains. While the solar-air temperature approach improved accuracy in estimating free heating potential, geographic and temporal variations in solar radiation data, as well as unpredictable weather patterns, could impact real-world application, requiring localized adjustments for optimal performance.
- While the solar-air temperature approach improved accuracy in estimating free heating potential, geographic and temporal variations in solar radiation data, as well as unpredictable weather patterns, could impact real-world application, requiring localized adjustments for optimal performance.

While higher solar absorptivity substantially enhances passive heating performance during winter, the present analysis does not address potential cooling penalties during summer months. Therefore, the findings should be interpreted strictly within the context of heating-dominated periods. Extending the methodology toward an integrated annual heating–cooling assessment represents an important direction for future work. Future research should focus on refining the solar-air temperature model by incorporating building-specific variables such as orientation, shading, and real-time solar radiation data. The proposed methodology represents an advancement over conventional heating degree-hour calculations by integrating solar-air temperature adjustments, thereby enhancing accuracy in estimating passive heating contributions. By identifying optimal heating hours (10:00 a.m. - 2:00 p.m.) and assessing case-specific material optimizations, the study provides a practical and replicable framework for reducing reliance on mechanical heating. The validation using real meteorological data underscores the applicability of the proposed method for diverse climate regions, ensuring its usability in sustainable building design and energy-efficient heating strategies. Additionally, expanding the methodology to other climate regions and integrating it with smart grid technologies will provide further insights into the potential of passive heating in diverse environmental conditions. This approach represents a significant step toward more sustainable and energy-efficient building design, aligning with global efforts to reduce carbon emissions and improve energy management.

CRediT authorship contribution statement

Ali Keçebaş: Writing – review & editing, Visualization, Software, Investigation, Conceptualization. **Hongwei Wu:** Writing – review & editing, Writing – original draft, Validation, Software, Formal analysis. **Mustafa Ertürk:** Validation, Resources, Methodology, Formal analysis, Data curation. **C Ahamed Saleel:** Writing – review & editing, Validation, Investigation, Formal analysis, Data curation.

Declaration of competing interest

The authors declare that they have no known competing financial interests or personal relationships that could have appeared to influence the work reported in this paper.

Acknowledgments

The authors extend their appreciation to the Deanship of Research and Graduate Studies at King Khalid University for funding this work through Large Research Project under grant number RGP2/354/46.

Nomenclature

A	surface area (m^2)
c	unit energy cost of fuel ($/kWh$m^2$year)
C	energy cost saving ($/$m^2$year)
CEF	carbon emission factor (ton CO_2/kWh)
$\dot{E}$	energy rate (kW)
FR	carbon footprint reduction (ton CO_2/m^2year)
h	heat transfer coefficient (W/m^2 K)
HDH	heating degree-hours (°h)
I	solar radiation (W/m^2)
$\dot{Q}$	heat rate (kW)
S	percentage energy saving (%)
t	time (h)
T	temperature (K)
U	total heat transfer coefficient (W/m^2 K)

Greek symbols

α	absorptivity
ε	emissivity
η	efficiency of heating system
σ	Stephane-Botzmann constant

Subscripts

amb	ambient
conv	convection
fh	free heating
max	maximum
min	minimum
o	overall
rad	radiation
sa	solar-air

Abbreviations

CDH	Cooling Degree-Hours
HDH	Heating Degree-Hours

Data availability

Data will be made available on request.

References

[1] K.K. Jaiswal, C.R. Chowdhury, D. Yadav, R. Verma, S. Dutta, K.S. Jaiswal, B. Sangmesh, K.S.K. Karuppasamy, Renewable and sustainable clean energy development and impact on social, economic, and environmental health, Energy Nexus 7 (2022) 100118, https://doi.org/10.1016/j.nexus.2022.100118.

[2] A.L. Alaoui, A. Amrani, A.A. Merrouni, J.E. Salhi, O. Boulerhcha, A. Daoudia, Y. El Hassouani, E. Chaabelasri, M. Halimi, Thermal and energy efficiency study of passive heating and cooling systems in Morocco's cold desert climate. e-Prime – adv. Electric. Eng. Electron, Energy 6 (2023) 100355, https://doi.org/10.1016/j.prime.2023.100355.

[3] M. Formolli, T. Kleiven, G. Lobaccaro, Assessing solar energy accessibility at high latitudes: a systematic review of urban spatial domains, metrics, and parameters, Renew. Sustain. Energy Rev. 177 (2023) 113231, https://doi.org/10.1016/j.rser.2023.113231.

[4] W. Cai, X. Wen, C. Li, J. Shao, J. Xu, Predicting the energy consumption in buildings using the optimized support vector regression model, Energy 273 (2023) 127188, https://doi.org/10.1016/j.energy.2023.127188.

[5] F.S. Hafez, B. Sa'di, M. Safa-Gamal, Y.H. Taufiq-Yap, M. Alrifaey, M. Seyedmahmoudian, A. Stojcevski, B. Horan, S. Mekhilef, Energy efficiency in sustainable buildings: a systematic review with taxonomy, challenges, motivations, methodological aspects, recommendations, and pathways for future research, Energy Strategy Rev. 45 (2023) 101013, https://doi.org/10.1016/j.esr.2022.101013.

[6] M. Seraj, M. Parvez, O. Khan, Z. Yahya, Optimizing smart building energy management systems through industry 4.0: a response surface methodology approach, Green Techn. Sustain. 2 (2) (2024) 100079, https://doi.org/10.1016/j.grets.2024.100079.

[7] M. Economidou, V. Todeschi, P. Bertoldi, D. D'Agostino, P. Zangheri, L. Castellazzi, Review of 50 years of EU energy efficiency policies for buildings, Energy Build. 225 (2020) 110322, https://doi.org/10.1016/j.enbuild.2020.110322.

[8] A. Veljkovic, D.A. Pohoryles, D.A. Bournas, Heating energy demand estimation of the EU building stock: combining building physics and artificial neural networks, Energy Build. 298 (2023) 113474, https://doi.org/10.1016/j.enbuild.2023.113474.

[9] B. Ozarisoy, Energy effectiveness of passive cooling design strategies to reduce the impact of long-term heatwaves on occupants' thermal comfort in Europe: climate change and mitigation, J. Clean. Prod. 330 (2022) 129675, https://doi.org/10.1016/j.jclepro.2021.129675.

[10] J. Zhang, L.J. Nilsson, Comparative analysis of energy efficient technology innovation in buildings: the case of passive houses in Germany, Sweden and China, in: T. Lindström (Ed.), ECEEE Summer Study Proceedings, vol. 2, European Council for an Energy Efficient Economy, 2013 (ECEEE).
[11] M. Ghamari, C.H. See, D. Hughes, T. Mallick, K.S. Reddy, K. Patchigolla, S. Sundaram, Advancing sustainable building through passive cooling with phase change materials, a comprehensive literature review, Energy Build. 312 (2024) 114164, https://doi.org/10.1016/j.enbuild.2024.114164.
[12] S. Jaouaf, B. Bensaad, M. Habib, Passive strategies for energy-efficient educational facilities: insights from a mediterranean primary school, Energy Rep. 11 (2024) 3653–3683, https://doi.org/10.1016/j.egyr.2024.03.040.
[13] M. Carpio, L.M. López-Ochoa, J. Las-Heras-Casas, K. Verichev, Influence of heating degree day calculation methods in designing the thermal envelope of buildings, J. Build. Eng. 46 (2022) 103604, https://doi.org/10.1016/j.jobe.2021.103604.
[14] S. Park, J. Shim, D. Song, Issues in calculation of balance-point temperatures for heating degree-days for the development of building-energy policy, Renew. Sustain. Energy Rev. 135 (2021) 110211, https://doi.org/10.1016/j.rser.2020.110211.
[15] Y. Pan, M. Zhu, Y. Lv, Y. Yang, Y. Liang, R. Yin, Y. Yang, X. Jia, X. Wang, F. Zeng, S. Huang, D. Hou, L. Xu, R. Yin, X. Yuan, Building energy simulation and its application for building performance optimization: a review of methods, tools, and case studies, Adv. Appl. Energy 10 (2023) 100135, https://doi.org/10.1016/j.adapen.2023.100135.
[16] A. Bolattürk, Optimum insulation thicknesses for building walls with respect to cooling and heating degree-hours in the warmest zone of Turkey, Build. Environ. 43 (2008) 1055–1064, https://doi.org/10.1016/j.buildenv.2007.02.014.
[17] J. Yu, L. Tian, C. Yang, X. Xu, J. Wang, Optimum insulation thickness of residential roof with respect to solar-air degree-hours in hot summer and cold winter zone of China, Energy Build. 43 (2011) 2304–2313, https://doi.org/10.1016/j.enbuild.2011.05.012.
[18] C. Aktemur, M.T. Çakır, M.F. Çakır, Optimising of thermal insulation thickness based on wall orientations and solar radiation using heating-degree hour method, Case Stud. Therm. Eng. 60 (2024) 104725, https://doi.org/10.1016/j.csite.2024.104725.
[19] E. Wati, P. Meukam, M.K. Nematchoua, Influence of external shading on optimum insulation thickness of building walls in a tropical region, Appl. Therm. Eng. 90 (2015) 754–762, https://doi.org/10.1016/j.applthermaleng.2015.07.052.
[20] Y. Zhou, C.W.F. Yu, G. Zhang, Study on heat-transfer mechanism of wallboards containing active phase change material and parameter optimization with ventilation, Appl. Therm. Eng. 144 (2018) 1091–1108, https://doi.org/10.1016/j.applthermaleng.2018.04.083.
[21] A.A. Alola, S.S. Akadiri, A.C. Akadiri, U.V. Alola, A.S. Fatigun, Cooling and heating degree days in the US: the role of macroeconomic variables and its impact on environmental sustainability, Sci. Total Environ. 695 (2019) 133832, https://doi.org/10.1016/j.scitotenv.2019.133832.
[22] W. He, C. Yu, J. Yang, B. Yu, Z. Hu, D. Shen, X. Liu, M. Qin, H. Chen, Experimental study on the performance of a novel RC-PCM-wall, Energy Build. 199 (2019) 297–310, https://doi.org/10.1016/j.enbuild.2019.07.001.
[23] L. Huang, Z. Zhai, Critical review and quantitative evaluation of indoor thermal comfort indices and models incorporating solar radiation effects, Energy Build. 224 (2020) 110204, https://doi.org/10.1016/j.enbuild.2020.110204.
[24] K. Panchabikesan, M.M. Joybari, F. Haghighat, V. Ramalingam, Y. Ding, Feasibility study on the year-round operation of PCM based free cooling systems in tropical climatic conditions, Energy 192 (2020) 116695, https://doi.org/10.1016/j.energy.2019.116695.
[25] D. Shen, C. Yu, W. Wang, Investigation on the thermal performance of the novel phase change materials wall with radiative cooling, Appl. Therm. Eng. 176 (2020) 115479, https://doi.org/10.1016/j.applthermaleng.2020.115479.
[26] A. Ustaoglu, K. Kurtoglu, A. Yaras, A comparative study of thermal and fuel performance of an energy-efficient building in different climate regions of Turkey, Sustain. Cities Soc. 59 (2020) 102163, https://doi.org/10.1016/j.scs.2020.102163.
[27] T. Yan, X. Xu, J. Gao, Y. Luo, J. Yu, Performance evaluation of a PCM-embedded wall integrated with a nocturnal sky radiator, Energy 210 (2020) 118412, https://doi.org/10.1016/j.energy.2020.118412.
[28] L. Yang, R. Fu, W. He, Q. He, Y. Liu, Adaptive thermal comfort and climate responsive building design strategies in dry–hot and dry–cold areas: case study in Turpan, China, Energy Build. 209 (2020) 109678, https://doi.org/10.1016/j.enbuild.2019.109678.
[29] C. Zhang, F. Xiao, J. Wang, Design optimization of multi-functional building envelope for thermal insulation and exhaust air heat recovery in different climates, J. Build. Eng. 43 (2021) 103151, https://doi.org/10.1016/j.jobe.2021.103151.
[30] H.M.F. Shakir, A. Ali, U. Zubair, T.Z.A. Zhao, Z.A. Rehan, I. Shahid, Fabrication of low emissivity paint for thermal/NIR radiation insulation for domestic applications, Energy Rep. 8 (2022) 7814–7824, https://doi.org/10.1016/j.egyr.2022.05.287.
[31] Y. Yang, S. Chen, Thermal insulation solutions for opaque envelope of low-energy buildings: a systematic review of methods and applications, Renew. Sustain. Energy Rev. 167 (2022) 112738, https://doi.org/10.1016/j.rser.2022.112738.
[32] F. Kheiri, J.S. Haberl, J.C. Baltazar, Split-degree day method: a novel degree day method for improving building energy performance estimation, Energy Build. 289 (2023) 113034, https://doi.org/10.1016/j.enbuild.2023.113034.
[33] G. Li, W. Tian, H. Zhang, X. Fu, A novel method of creating machine learning-based time series meta-models for building energy analysis, Energy Build. 281 (2023) 112752, https://doi.org/10.1016/j.enbuild.2022.112752.
[34] M. Sulzer, A. Christen, A. Matzarakis, Predicting indoor air temperature and thermal comfort in occupational settings using weather forecasts, indoor sensors, and artificial neural networks, Build. Environ. 234 (2023) 110077, https://doi.org/10.1016/j.buildenv.2023.110077.
[35] R.Y.M. Wong, C.Y. Tso, S.Y. Jeong, S.C. Fu, C.Y.H. Chao, Critical sky temperatures for passive radiative cooling, Renew. Energy 211 (2023) 214–226, https://doi.org/10.1016/j.renene.2023.04.142.
[36] M. Fellah, S. Ouhaibi, N. Belouaggadia, K. Mansouri, H. Naji, Thermal insulation and energy performance's assessment of a mycelium-based composite wall for sustainable buildings, Case Stud. Constr. Mater. 20 (2024) e02786, https://doi.org/10.1016/j.cscm.2023.e02786.
[37] M.K. Ozturan, A.K. Seyhan, Determination of optimum insulation thickness of building walls according to four main directions by accounting for solar radiation: a case study of Erzincan, Türkiye, Energy Build. 304 (2024) 113871, https://doi.org/10.1016/j.enbuild.2023.113871.
[38] R.M. Palma, D.C. Medina, M.G. Delgado, J.S. Ramos, P. Montero-Gutierrez, S.A. Domínguez, Enhancing the building resilience in a changing climate through a passive cooling roof: a case study in Camas (Seville, Spain), Energy Build. 321 (2024) 114680, https://doi.org/10.1016/j.enbuild.2024.114680.
[39] A. Breteau, E. Bozonnet, P. Salagnac, J.M. Caous, Specific metrics for direct adiabatic cooling of industrial buildings and climate adaptation, Energy Build. 332 (2025) 115472, https://doi.org/10.1016/j.enbuild.2025.115472.
[40] G. Gianpiero Evola, A. Andrea Longhitano, V. Vincenzo Costanzo, F. Francesco Nocera, Application of synthetic indices for thermal discomfort assessment in historical buildings according to the adaptive approach, Energy Build. 336 (2025) 115648, https://doi.org/10.1016/j.enbuild.2025.115648.
[41] S. Fan, T. Yan, L. Che, J. Liu, X. Li, W. Lyu, X. Xu, An energy saving potential evaluation method of a pipe-embedded wall integrated with natural energies, Renew. Energy 238 (2025) 121930, https://doi.org/10.1016/j.renene.2024.121930.
[42] M. Fellah, S. Ouhaibi, N. Belouaggadia, K. Mansouri, Harnessing machine learning for enhanced thermal insulation and energy efficiency in buildings worldwide, Results Eng. 25 (2025) 104086, https://doi.org/10.1016/j.rineng.2025.104086.
[43] S. Zhou, C. Chang, K. Shan, C. Wang, X. Guo, M. Song, Q. Wu, A climate adaptability investigation of a novel double-skin wall incorporating phase change materials during wintertime, Renew. Energy 239 (2025) 122105, https://doi.org/10.1016/j.renene.2024.122105.
[44] R. Zmeureanu, H. Dou, H. Ge, L. Wang, Z. Xie, Thermal time constant estimation of unoccupied school buildings from field measurements over summer, J. Build. Eng. 104 (2025) 112311, https://doi.org/10.1016/j.jobe.2025.112311.
[45] C. Ghiaus, Equivalence between the load curve and the free-running temperature in energy estimating methods, Energy Build. 38 (2006) 429–435, https://doi.org/10.1016/j.enbuild.2005.08.003.
[46] M. De Rosa, V. Bianco, F. Scarpa, L.A. Tagliafico, Heating and cooling building energy demand evaluation; a simplified model and a modified degree days approach, Appl. Energy 128 (2014) 217–229, https://doi.org/10.1016/j.apenergy.2014.04.067.
[47] L.D.D. Harvey, Using modified multiple heating-degree-day (HDD) and cooling-degree-day (CDD) indices to estimate building heating and cooling loads, Energy Build. 229 (2020) 110475, https://doi.org/10.1016/j.enbuild.2020.110475.
[48] W. Lyu, X. Li, W. Shi, B. Wang, X. Huang, A general method to evaluate the applicability of natural energy for building cooling and heating: revised degree hours, Energy Build. 250 (2021) 111277, https://doi.org/10.1016/j.enbuild.2021.111277.

[49] Y. Zhang, K. Lin, Q. Zhang, H. Di, Ideal thermophysical properties for free-cooling (or heating) buildings with constant thermal physical property material, Energy Build. 38 (2006) 1164–1170, https://doi.org/10.1016/j.enbuild.2006.01.008.
[50] I. Pothof, D. Vreeken, M. van Meerkerk, Data-driven method for optimized supply temperatures in residential buildings, Energy 284 (2023) 129183, https://doi.org/10.1016/j.energy.2023.129183.
[51] G.R. Roshan, A.A. Ghanghermeh, S. Attia, Determining new threshold temperatures for cooling and heating degree day index of different climatic zones of Iran, Renew. Energy 101 (2017) 156–167, https://doi.org/10.1016/j.renene.2016.08.053.
[52] X. Huo, L. Yang, D.H.W. Li, Y. Zhai, S. Lou, A novel index for assessing the climate potential of free-running buildings based on the acceptable upper limits of thermal comfort models across China, Energy Convers. Manag. 278 (2023) 116692, https://doi.org/10.1016/j.enconman.2023.116692.
[53] C. McGilligan, S. Natarajan, M. Nikolopoulou, Adaptive comfort degree-days: a metric to compare adaptive comfort standards and estimate changes in energy consumption for future UK climates, Energy Build. 43 (2011) 2767–2778, https://doi.org/10.1016/j.enbuild.2011.06.037.
[54] J. Hu, Y. He, Q. Wang, B. Wang, X. Hao, N. Li, W. Yin, L. Liu, Resilient or resistant to non-neutral environments? A comparative study on occupant thermal needs in buildings under natural ventilation, fee-free heating, and fee-charged heating modes, J. Build. Eng. 72 (2023) 106651, https://doi.org/10.1016/j.jobe.2023.106651.
[55] A. Keçebaş, H. Gökgedik, E.Y. Gürbüz, M. Ertürk, Energy and exergy-based degree-hours in estimation of heat requirements for heating and cooling purposes, Energy Convers. Manag. 307 (2024) 118347, https://doi.org/10.1016/j.enconman.2024.118347.
[56] G. Karaca-Dolgun, A. Keçebaş, M. Ertürk, A. Daşdemir, Life cycle cost assessment for thermal insulation of above-ground spherical container with different capacities in hot fluid storage processes, J. Clean. Prod. 403 (2023) 136875, https://doi.org/10.1016/j.jclepro.2023.136875.
[57] ISO 13790 standard, Energy performance of buildings - calculation of energy use for space heating and cooling, ISO 13790, https://www.iso.org/standard/41974.html#:~:text=ISO%2013790%3A2008%20gives%20calculation,to%20as%20%E2%80%9Cthe%20building%E2%80%9D, 2008.
[58] Y.A. Çengel, S. Klein, W. Beckman, Heat Transfer: a Practical Approach, McGraw-Hill, New York, USA, 1998.
[59] ISO 6946, Building Components and Building Elements-Thermal Resistance and Thermal Transmittance, International Organization for Standardization, Geneva, 2017.
[60] ASHRAE, ASHRAE Handbook-Fundamentals, American Society of Heating, Refrigerating and Air-Conditioning Engineers, Atlanta, GA, 2017.
[61] General Directorate of Meteorology, General Directorate of Meteorology, 2024. Turkey, https://www.mgm.gov.tr/. July 2024.
[62] A.S. Canbolat, An integrated assessment of the financial and environmental impacts of exterior building insulation application, J. Clean. Prod. 435 (2024) 140376, https://doi.org/10.1016/j.jclepro.2023.140376.